The Thesis Committee for Mignon Denise Fitzpatrick
Certifies that this is the approved version of the following thesis:

Microfabricated Environments for the Study of Bacterial Group Behavior

APPROVED BY
SUPERVISING COMMITTEE:

Supervisor:

Jason B. Shear

Marvin Whiteley

Microfabricated Environments for the Study of Bacterial Group Behavior

by

Mignon Denise Fitzpatrick, B.S.

Thesis

Presented to the Faculty of the Graduate School of

The University of Texas at Austin

in Partial Fulfillment

of the Requirements

for the Degree of

Master of Arts

The University of Texas at Austin

December 2015

Acknowledgements

I would first and foremost like to thank my advisor Dr. Jason Shear for the direction, encouragement, and understanding he has given me both as an undergraduate and subsequently as graduate student. I appreciate the opportunity he has given me to be a part of the Shear lab, an environment which encourages both creativity and individuality and has taught me perseverance in the face of obstacles. I would also like to thank Marvin Whitely, whose invaluable insight and enthusiasm has been an inspiration. In addition, I would like to thank former lab members Drs. Jodi Connell and Eric Ritschdorff for their contribution to this research, and the great deal of time and effort they spent helping me to become a better scientist. In addition, I owe thanks to former lab members Drs. Eric Spivey, Todd Hoppe, Mike Robinson, Maryam Ali, and Derek Hernandez, as well as current lab members Janine Elliott, Olja Simoska, and especially Allison Myers, for their help, advice and companionship. I would like to thank Drs. Aimee Wessel and Sophie Darch from the Whiteley lab, as well as Talha Arshad from the Bonnecaze lab, for their contribution to this research. In addition, I would like to thank Tim Hooper for his assistance with broken equipment, Dr. Julie Hayes for her help with confocal microscopy, and Betsy Hamblen for her unwavering support and positivity. I am also grateful for the funding provided for this research from the Army Research Office and the Welch Foundation.

I would also like to thank my parents, Michael and Maureen Fitzpatrick, along with my brothers Sean and Aaron, for their continued support and encouragement. In addition, I thank all of my friends, in particular Jeremy Madison, for supporting my goals and being a stabilizing force.

Abstract

Microfabricated Environments for the Study of Bacterial Group Behavior

Mignon Denise Fitzpatrick, M. A.

The University of Texas at Austin, 2015

Supervisor: Jason B. Shear

This thesis describes the application of micro three dimensional printing (μ3DP) techniques to create protein microstructures for the study of bacterial group behavior in small populations. Studies involving aggregates of ~10^1 to ~10^5 cells have shown extensive and complex communication and spatial organization. Multiphoton lithography (MPL) provides a means to quickly design and execute the fabrication of microscale structures with submicron resolution from a variety of biocompatible polymers. Using this technique, intricate spatial arrangements of bacteria can be achieved while maintaining small population sizes at high cell density ($\geq 10^8$ cells mL^{-1}), providing *in vitro* culture conditions which better simulate *in vivo* settings. As a result, valuable information can be obtained about bacterial social interactions through the coupling of additional analytical techniques to detect the presence or absence of extracellular signaling molecules. While quorum sensing (QS) remains the most extensively studied means of bacterial communication, it is becoming increasingly apparent that additional factors are necessary to effect certain changes in population-wide genetic expression which can lead to increased virulence,

pathogenicity, and the development of antibiotic resistance. The work presented in this thesis addresses the influences of cell density, chemical heterogeneity of the environment within cell aggregates, and level of cell surface attachment as mechanisms to induce or influence the development of antibiotic resistance. Building upon previous work presented by members of the Shear lab, BSA-gelatin protein microstructures were used to study the behavior and response of the opportunistic pathogen *Pseudomonas aeruginosa* under these conditions. Antibiotic resistance was observed in low cell number/high density populations in agreement with previous work presented by the Shear lab. In addition, it was found that localized regions of oxygen depletion do not correlate directly with antibiotic resistance development, as the population size required for depletion far exceeded that for development of resistance. Finally, a new technique directed at simultaneous biofilm inhibition and cell removal from solution was explored.

Table of Contents

List of Figures

Chapter 1: Introduction

1.1 The Study of Bacterial Populations -- A Changing Landscape

In recent years, it has become evident that studying the social behavior of microorganisms can provide vital information with respect to how bacteria are able to develop antibiotic resistance and thrive in infection settings [1]–[5]. Opportunistic pathogens such as Gram (-) *Pseudomonas aeruginosa*, which frequently infects humans as a result of hospital acquired infections or immune compromising diseases like cystic fibrosis (CF), have been shown to communicate extensively within a population [6][7]. This communication is known to be, at least in part, facilitated through the use of small signaling molecules in a process known as quorum sensing (QS) [8][9]. Despite the progress in understanding this fundamental means of communication, however, there are many other potential factors in the development of resistance that remain to be discovered.

Recent studies have emphasized the importance of small aggregate formation and bacterial spatial organization as being fundamental to the survival of bacteria within the polymicrobial environments that characterize chronic wounds and other infection sites [10]–[12]. Many current technologies being used to study bacterial behavior lack the ability to mimic these small aggregate population sizes and densities, and limit the ability to design complex polymicrobial colonies [13]. In addition, it can be difficult to isolate and grow truly monoclonal populations of cells, which have certain advantages in genetic analyses such as RNA sequencing [14]. As a result, the Shear lab has developed multiphoton lithography (MPL) techniques for fabrication of three-dimensional (3D) biocompatible microstructures around individual cells [15]–[17]. The ability to design and execute the fabrication of these arbitrary 3D structures around cells on a timescale of minutes, combined with the tunable nature of a protein hydrogel matrix and the potential to retrieve

intact structures for sequencing makes this technique highly applicable in the field of sociomicrobiology. In addition, the coupling of these structures to existing analytical techniques such as scanning electrochemical microscopy (SECM) has already proven effective, and transparent carbon ultramicroelectrode arrays (T-CUAs) have been developed and characterized with the goal of integrating spectroelectrochemical analysis [18]–[20].

The topics covered in this thesis investigate various aspects of bacterial group behavior using 3D microstructures, such as those presented in Figure 1.1, to achieve various cellular densities, population sizes, and configurations. The data presented here serve as a foundation for further studies in the determination of how cellular organization within small populations is integral to the development of antibiotic resistance.

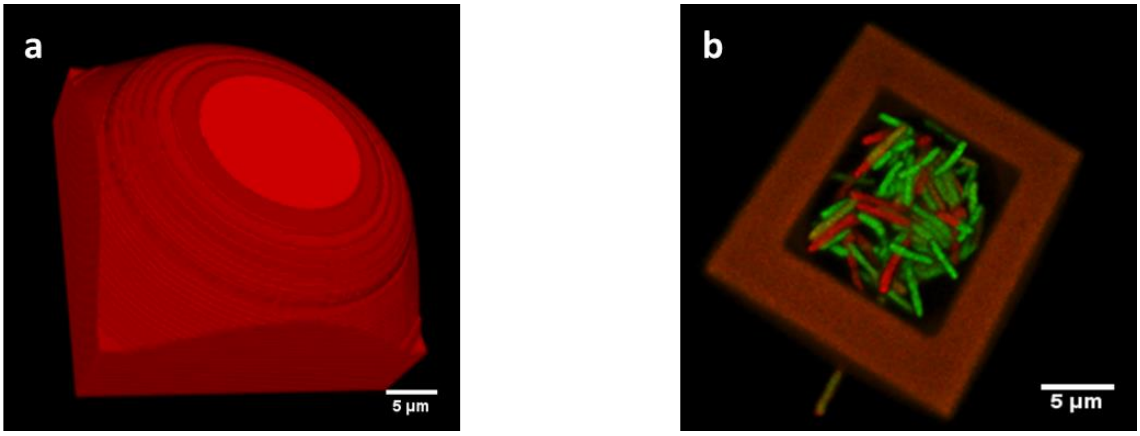

Figure 1.1 Bacterial microtraps used for studying small populations. (a) 3D reconstruction of a microstructure design mask. (b) Confocal image of a microstructure (orange) containing live (green) and dead (red) P. aeruginosa following dosing with gentamicin.

1.1.1 Bacterial Group Behavior

The environment and organization of bacterial communities can be intricate and complex. At the microlevel, populations can self-organize, forming various three-

dimensional architectures of cells and extracellular matrix (ECM) [10]. These aggregates can vary in cell number, density, and structure depending on cell type [21]. In addition, environmental stressors and communication between cells of the same species as well as other species nearby can have an effect. Communication can also induce changes in gene expression and resultant phenotype. This in turn can trigger the production of ECM to provide scaffolding for the aggregate, increase virulence, or assist in enabling the development of antibiotic resistance, among other responses. Conversely, if communication (or lack thereof) indicates the need for down-regulation of genes that direct aggregate formation, cells can disperse and redirect their energy expenditures [22]–[25] [26].

The most commonly studied means of communication/response within and amongst bacterial populations is quorum sensing (QS). QS refers to the production of small signaling molecules, which can be secreted and recognized by other cells nearby [9]. As population density increases, the extracellular concentration of signal molecules begins to increase. When cells detect a threshold level of signal, they respond by increasing signal production in a positive feedback loop. At high levels, this process results in population-wide changes in genetic expression (Figure 1.2a), which favors interaction and cooperation within the growing aggregate, and can often result in increased pathogenicity [2][22] [24][27].

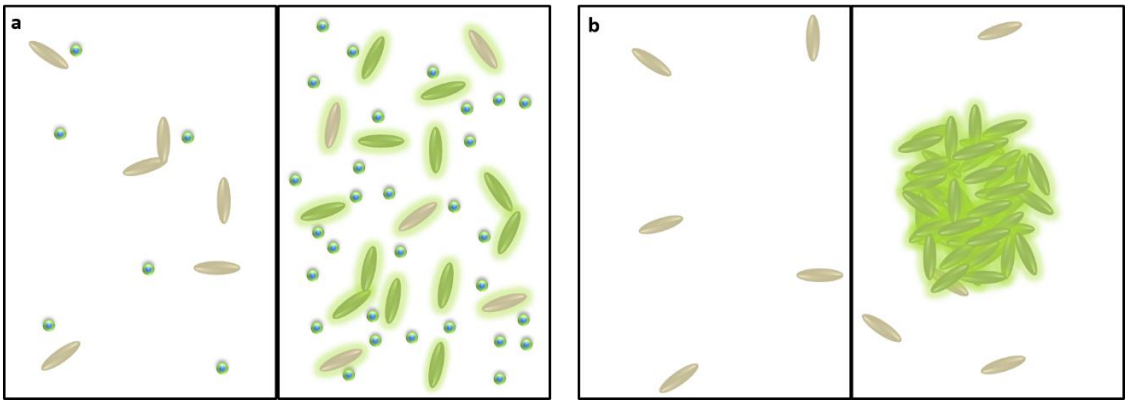

Figure 1.2 Communication between cells affects genetic expression of the population. (a) Low concentration of autoinducer (blue) does not affect genetic expression of a low density population of cells (beige; left), while a higher concentration in a denser population causes a change (green; right). (b) lack of physical contact in low density population of cells (left) does not induces genetic change, while close contact within a high density population does (right).

Such group, or "social," behavior is not limited to cells within a particular aggregate, however. The pathogenicity and survival of a community of multiple aggregates relies on both intra- and inter-species communication to facilitate necessary spatial organization and matrix composition [23][28]–[30]. Dynamic modifications in aggregate size and three-dimensional organizations have been observed in response to the presence and proximity of other aggregates. Various autoinducers, while generally species-specific, can serve as indicators for the presence of a foreign species [31]. Bacteria have also been shown to produce their own antimicrobials to prevent the encroachment of other species [32]. Furthermore, competing species will occasionally use a compound approach to keep each other at specific distances by producing metabolites that result in different qualitative effects at different positions along a concentration gradient [25]. As a result, it is becoming increasingly necessary to develop platforms for creating and characterizing specific, well-defined structural organizations of small, dense polymicrobial communities, where

characterizations may include various methodologies, including microscopic and analytical sensing techniques.

1.1.2 Historical Techniques and Moving Forward

Some of the most fundamental early advances made in bacterial culture techniques can be attributed to Louis Pasteur and Robert Koch over a century ago. They provided a means to study and culture individual strains of bacteria, without which modern microbiology could not have developed [33]. Flask and plate culture still provides the foundation upon which most modern microbiology labs rely [9]. However, these techniques are hardly suitable to provide information about the complex interactions and spatial organizations within microbial communities *in vivo*. Moreover, it has been shown that cells grown using common culture environments such as a flask tend to be limited to densities $<10^9$ cells mL^{-1}, much lower than those found in aggregates, which can be as high as $\sim10^{12}$ cells mL^{-1} [9][34]. It also becomes difficult to achieve and maintain well-defined small population sizes. Cell clusters ranging from $\sim10^1$ to $\sim10^5$ cells have been shown to be important in pathogenicity, sizes which are difficult to organize and maintain using conventional culture technologies [35]–[37]. Such shortcomings indicate a need for a more sophisticated means of bacterial culture in the lab.

Recently, there has been a burgeoning development in the field of microfluidics and microdroplet approaches intended to at least partially address some of these limitations [14][38] [39]. Both of these sets of techniques allow for the isolation of small aggregates within defined chemical environments as well as coupling with additional analytical techniques [40]–[43]. However, both also fall short in providing the means necessary to facilitate defined, sustainable polymicrobial environments, and lack the ability to serve as dynamic platforms for bacterial cell culture.

1.1.3 A Solution in Micro 3D Printing

In response to the dearth of culture techniques allowing for precise structural arrangement and complexity of microenvironment observed *in vivo*, the Shear lab has continued to optimize the technique of protein multiphoton lithography (MPL) as a means of generating these conditions. The dynamic mask-based form of MPL, referred to as micro three dimensional printing (μ3DP) in the Shear lab, allows for rapid prototyping, enabling the design and construction of protein microstructures such as the one displayed in Figure 1.3 on the timescale of minutes [15][44][45]. These protein hydrogels have been shown to be biocompatible, tunable with respect to diffusion properties and stiffness, and can be designed to feature regions of immobilized biologically relevant chemicals or biomolecules [16][46]–[48]. Some modifications are introduced prefabrication as in the case of conjugating peptides to the protein reagents before fabrication, or adjusting protein concentrations to influence crosslinking density[47]. Other modifications are made post-fabrication, such as light induced swelling and creating variable substrate patterning through additional laser scans [49].

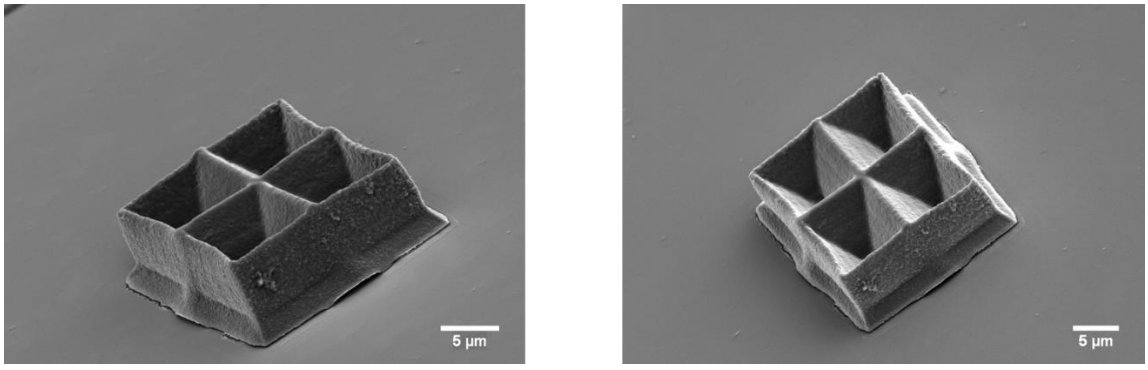

Figure 1.3 Scanning electron micrographs from two different angles of a protein microstructure created with μ3DP. Structure contact with the coverslip was broken as a result of sample preparation for electron microscopy, and is not representative of normal contact.

These capabilities provide the opportunity to design and modify microbial environments in order to achieve more suitable culture conditions. Adjustments can be made to the melting point of the protein solution by adding or modifying gelatin concentration, providing the ability to fabricate in situ around stationary cells [17][50]. Multi-step fabrication allows for the entrapment of multiple species of bacteria within nested structures, and differential growth times can allow the respective species to achieve relevant aggregate sizes and densities [17]. This technique also has potential applications in culturing "unculturable" bacterial strains, as the structures can be used to isolate monoclonal populations while allowing the reintroduction of the liquid matrix from which the isolate originated, including other microorganism species [51][52]. In addition, these microstructures are recoverable, and large numbers of structures can be concentrated and reclaimed, providing valuable information for genetic sequencing.

Another key advantage of combining μ3DP with cell culture is that the approach can be coupled with additional analytical techniques. Recently, it was shown that scanning electrochemical microscopy (SECM) could be effectively coupled with this type of culture to perform real time, in situ detection of pyocyanin, a toxin produced by *Pseudomonas aeruginosa* during the course of an infection [18][19]. Additionally, transparent carbon ultramicroelectrode arrays (T-CUAs) have been designed to couple with μ3DP cell culture to detect reactive oxygen species produced by *Streptococcus* species as an antimicrobial for other cell types [20][29][32].

1.2 MPE AND MPL

The numerous capabilities and advantages presented by μ3DP with respect to improving bacterial culture conditions inherently rely on the ability to achieve multiphoton excitation (MPE) and in its application to multiphoton lithography (MPL). The description

of multiphoton absorption theory by Maria Goeppert-Mayer in 1931 laid the groundwork for what would later be experimentally shown in the form of two-photon excitation (TPE) [53][54]. The following sections present an overview of MPE, including TPE, and subsequently how it is applied in MPL.

1.2.1 MPE

Prior to the theory presented by Maria Goeppert-Mayer, transition of an electron from the ground state to an excited state as a result of photonic absorption was considered to be linearly correlated with the energy of an incident photon [55]. Thus, the energy of one incident photon, if equal to the energy gap of the electronic transition within a chromophore, would promote excitation of one electron. Finally, either directly or following vibrational relaxation, a single photon of lesser energy would be emitted. However, Goeppert-Mayer predicted that two-photon absorption could occur under certain conditions, and decades later this was demonstrated using laser light as an excitation source [53][54]. In TPE, excitation occurs when the energy gap between two electronic states is bridged by the near-simultaneous absorption of two photons whose combined energies equal the energy necessary for an electronic transition. Upon the absorption of the first photon by a chromophore, one electron is promoted to a “virtual state”; a second photon must be absorbed almost immediately (on the order of femtosecond timescales) to prevent relaxation of the electron via scattering. In such an instance, two incident photons of longer wavelength and lower energy can result in an energy transition that is double their individual magnitudes. These concepts are illustrated in Figure 1.4.

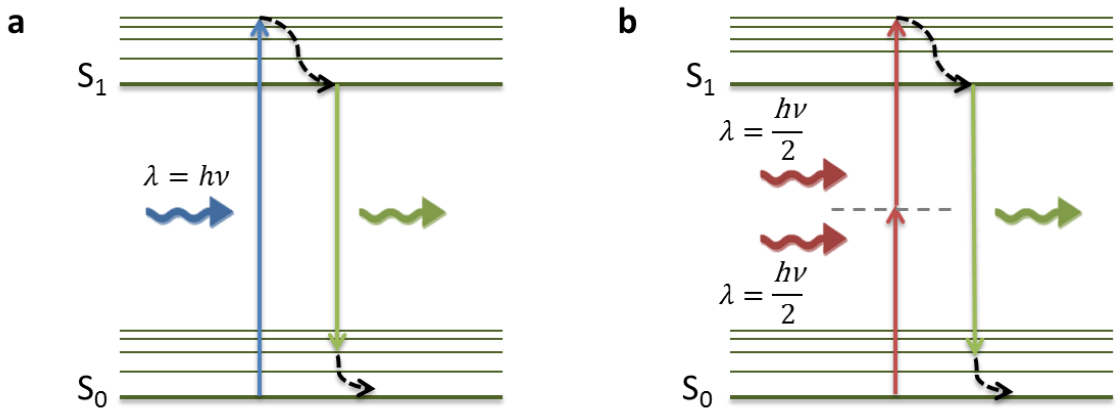

Figure 1.4 Jablonski diagrams for single-photon and two-photon excitation. (a) One photon excitation (1PE) occurs where one high frequency (e.g., "blue") photon is absorbed, followed by an electronic transition, and a lower wavelength (e.g., "green") photon is emitted. (b) TPE occurs where two low frequency (e.g., "red") photons are absorbed, followed by an electronic transition occurring through the virtual state and a lower wavelength green photon is emitted.

Due to the limited lifetime of this virtual state, the excitation photon flux must be extremely high in order to achieve practical levels of MPE events. It is convenient to consider the TPE of a chromophore as analogous to a chemical reaction in which M is the chromophore, M* is the excited chromophore, hν is a photon and n is the number of absorbed photons required to reach the excited state [56]:

$$M + n(h\nu) \leftrightarrow M^* \qquad [1.1]$$

Thus the reaction "rate" can be described using the following equation:

$$\frac{dM^*}{dt} = k\,[h\nu]^n[M] = \delta I^n[M] \qquad [1.2]$$

Here, k is the rate constant, I (photons s^{-1} cm^{-2}) is the instantaneous intensity of the excitation source, and δ ($cm^{2n}(s/photon)^{n-1}$) is the excitation cross-section. As a result, the rate of one photon excitation (1PE) scales linearly with intensity as demonstrated in

Equations 1.3 and 1.4, while in MPE the rate scales to the power of n as demonstrated in Equations 1.5 and 1.6.

$$M + 1(h\nu) \leftrightarrow M^* \quad [1.3]$$

$$\frac{dM^*}{dt} \propto I \quad [1.4]$$

$$M + 2(h\nu) \leftrightarrow M^* \quad [1.5]$$

$$\frac{dM^*}{dt} \propto I^2 \quad [1.6]$$

As such, high intensities are required to achieve MPE. Although the probability of near-simultaneous absorption of multiple photons is low, it can be increased by "focusing" photons into discrete temporal packets through the use of a femtosecond pulsed laser, and spatially focusing the laser light to very small dimensions (e.g., submicrometer beam waists) using high numerical aperture (NA) objectives. Such an approach can create a regime where planes nearest to the focal point support significant two-photon events, particularly for chromophores having relatively large two-photon absorption cross sections [56][57][58]. With appropriate optics, this three-dimensional area of excitation, or focal volume (voxel) can be confined to dimensions of ~1 μm^3, where the axial dimensions slightly exceed the radial (Figure 1.5) [56]. In addition, quality optics allow for the achievement of high instantaneous intensities at low average powers using a near infrared (NIR) tuned femtosecond laser such as a solid state titanium sapphire (Ti:S) laser. Typically, with an 80 MHz repetition rate and a low duty cycle of $\sim 10^{-5}$, such a laser in conjunction with high NA objectives can produce instantaneous intensities on the order of $\sim 10^{11}$ W cm^{-2} within the focal volume at an average power of only 10 mW [59].

Figure 1.5 Localization of excitation energy with MPE. (a) 1PE of a chromophore within solution results in excitation that occurs equally in all planes along the optical axis. (b) MPE allows focused excitation of a chromophore in solution, confined to small voxels centered near the focal point.

1.2.2 MPL

Multiphoton excitation is fundamental to the technique of multiphoton lithography and the inherent three-dimensional resolution of the process [60]. While MPL has been shown to form quality 3D microstructures from synthetic materials such as acrylate or epoxy polymers, the ability to engineer protein structures provides considerable advantages with respect to cell culture [61][62]. In order to fabricate solid protein matrices from liquid (or gelled) solutions, multiple inter-molecular crosslinking events must occur between side chains of amino acid residues of proteins in solution. This crosslinking tethers protein molecules to each other in a three-dimensional solid porous architecture [63]–[65]. Such a process is known to happen naturally in certain highly photo-oxidizable residues such as tyrosines, histidines, and tryptophans upon the exposure to UV light [66]. Alternatively, two-photon protein photocrosslinking can be accomplished with a high peak power mode-locked Ti:S laser, tuned to near IR wavelengths, and the help of a photosensitizer [67]. In this system a photosensitizer, such as Rose Bengal (Figure 1.6), undergoes MPE and facilitates the side chain crosslinking reactions via Type I or Type II mechanisms [68]. Type I processes result in the excitation of electrons in the photosensitizer to a triplet state, allowing direct interaction with the photo-oxidizable amino acid side chains. Following hydrogen abstraction, various free radical species become available to participate in the

crosslinking events [69]. In a Type II process (undergone by Rose Bengal), the photosensitizer is excited to a triplet state but then transfers energy to ground state molecular oxygen, producing singlet oxygen ($^1O_2$) that can in turn interact with protein side chains [70].

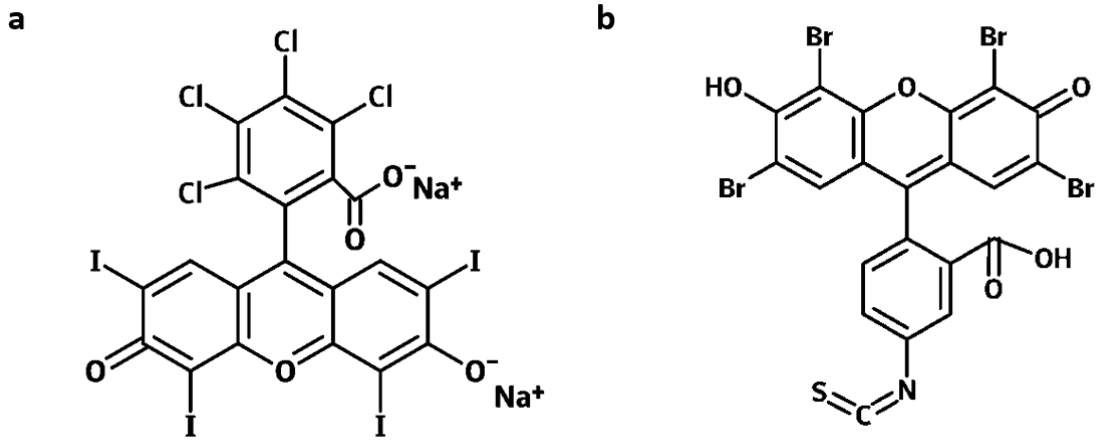

Figure 1.6 Molecular structure of two photosensitizers used in MPL. (a) Rose Bengal sodium salt. (b) Eosin isothiocyanate.

This crosslinking technique has been shown to be effective with different types of proteins, heterogeneous mixtures of proteins, and a variety of photosensitizers [17]. Additionally, MPL can be performed using proteins or polypeptides that have been conjugated to photosensitizers, such as eosin conjugated gelatin. This conjugation step helps diminish potential damage to cells by reducing cellular uptake of photosensitizer and further localizing reaction volumes.

The excitation volume is dependent on the focus achieved by the Ti:S and the table optics, and is optimally less than ~1 μm^3 [56][57][59]. The laser focus can then be translated through reagent solution, resulting in local excitation and reaction events that produce a solid crosslinked protein hydrogel. This focused beam can be raster-scanned in

the xy plane using dual axis galvo scanning mirrors, enabling fabrication at any position within the focal plane. To achieve fabrication patterns within the focal plane of the sample, a mask directed MPL technique is used which allows for a great deal of design flexibility. Here the laser is focused on a digital micromirror device (DMD) in a focal plane conjugate to that of the sample plane. In our system, the DMD is composed of an 800 x 600 array of individually addressable 16-μm x 16-μm aluminum mirrors that can be switched "on" or "off" by means of a ±10º tilt. Binary images containing black and white pixel arrays can be sent to the DMD using a computer, with white pixels resulting in the "on" state, allowing laser light to continue along the optical path towards the sample (Figure 1.7), and black pixels resulting in the "off" state, directing laser light away from the sample and into a beam block. As new image sequences are presented to the DMD and scanned in the sample image plane, the sample can be translated in the z-axis with the use of a motorized focus driver, enabling the fabrication of arbitrary three-dimensional structures with submicron resolution [15][45].

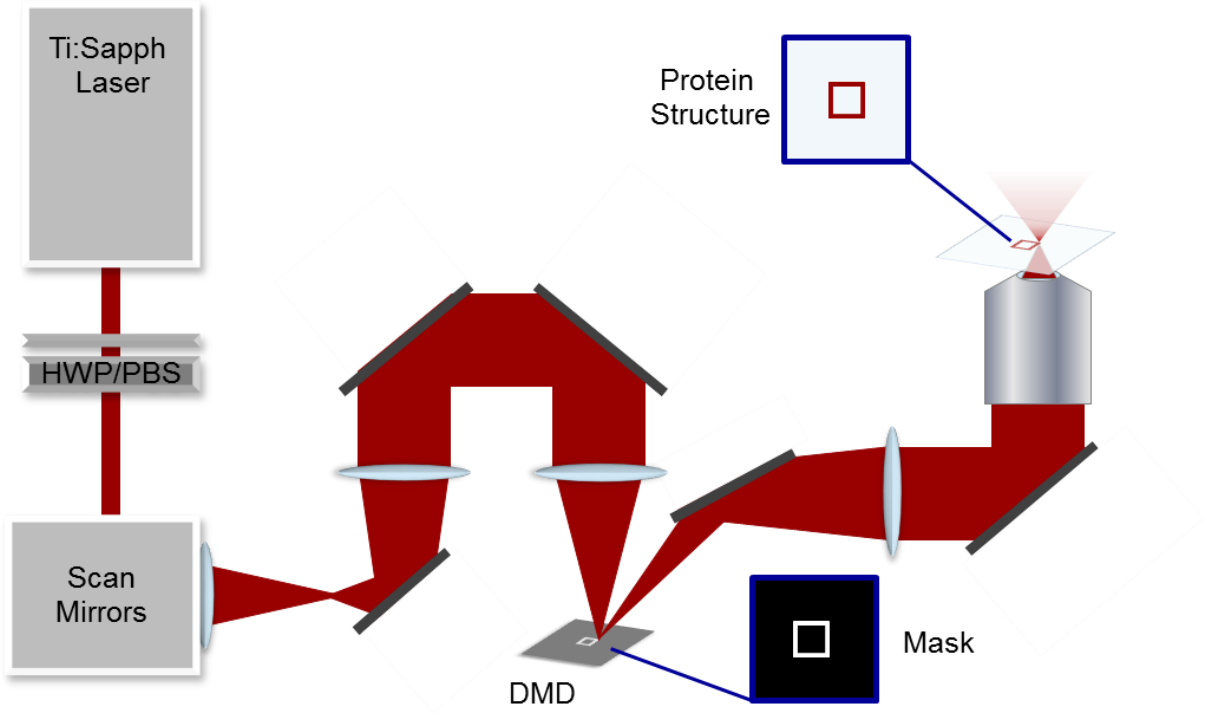

Figure 1.7 Mask-directed MPL. Attenuation of the Ti:S beam is accomplished with a combination half-waveplate/polarizing beam-splitting cube (HWP/PBS). The focused beam is then scanned by the pair of galvo-driven mirrors onto the digital micromirror device (DMD), which is in a plane conjugate to the sample focal plane determined by the objective. The mask indicates white "on" pixels of the DMD that reflect the beam into the objective, allowing fabrication of the protein structure indicated by the red square.

Chapter 2: Antibiotic Resistance and Cell Density

2.1 Introduction

The information presented in this chapter provides important observations about gelatin containing microstructures that can be referenced in the design and execution of future experiments. These studies are performed using *Pseudomonas aeruginosa*, an important model organism used extensively in research concerning hospital acquired infections, many of which result in highly antibiotic resistant populations [71][72][73]. It is important to understand the nature of how this resistance develops and be able to isolate contributing factors. Protein microstructures provide the opportunity to study small, clinically relevant populations (~10^1 to ~10^5 cells), and the use of a protein/gelatin mixture imparts high flexibility to cellular containers, allowing the structures to stretch as population size increases [17][74]. This enables the formation of maximally dense (~10^{12} cells mL^{-1}) pockets of viable cells, which is something that other techniques cannot achieve [34]. Determining how and at what density these pockets begin to develop antibiotic resistance is integral to learning how to prevent their formation [22][75]. Previous studies have shown a lack of definitive, precise correlation between onset of quorum sensing and the development of antibiotic resistance in small populations (~10^2 cells) [16][73]. It has been shown, however, that antibiotic resistance is correlated to population density [16]. As such, some method of communication between cells within a population must be occurring in order to induce the genetic changes necessary for this to occur [7]. In order to begin investigating this process, it is first necessary to ensure that the platform being used is effective and corresponds with existing data in the field. The information in this chapter was modeled to replicate previous experiments performed by the Shear lab in which antibiotic resistance was assessed at varying population densities in BSA-based

microstructures [16]. The following research was performed with the intent to support the use of gelatin containing microstructures in future antibiotic resistance studies.

2.2 Experimental Methods

2.2.1 Reagents

Bovine serum albumin (BAH64-0100) was purchased from Equitech-Bio (Kerrville, TX). Rose Bengal (330000) and Gelatin Type A from porcine, 300 Bloom (G-2500) were acquired from Sigma-Aldrich (St. Louis, MO), while Gelatin Type A from porcine, 60 Bloom (16560) was acquired from Electron Microscopy Sciences (Hatfield, PA). HEPES sodium salt (AC21500-1000) and propidium iodide (440300250) were obtained from Acros Organics (Geel, Belgium). Sodium chloride (S271-3) and carbenicillin disodium salts (BP2648-1) were purchased from Fisher BioReagents (Fairlawn, NJ). Tryptic soy broth (R455052) and tryptic soy agar (1.05458.0500) were obtained from Remel Thermo Scientific (Waltham, MA) and EMD Millipore (Billerica, MA), respectively.

2.2.2 Bacterial Strains, Plasmids and Culture Conditions

All experiments in this chapter were performed using a strain of *Pseudomonas aeruginosa* provided by the Whiteley lab: PA01 transfected with the *gfp* containing plasmid pMRP9-1 and a carbenicillin resistance marker. Plasmid maintenance was ensured during plate growth on tryptic soy agar (TSA) by using 100 $\mu g\ mL^{-1}$ carbenicillin. Cultures used in the fabrication process were started from a plate and incubated at 37°C overnight under aerobic conditions in tryptic soy broth (TSB). These were subsequently diluted in fresh TSB and grown to mid-logarithmic phase before dilution into the fabrication solution.

2.2.3 Protein Hydrogel Fabrication

A hydrogel precursor solution was created by first solubilizing Rose Bengal (RB) in TSB at 60ºC in a sonicating bath for one hour, followed by the addition of bovine serum albumin (BSA) and gelatin from porcine Type A 60 bloom (gelatin), which were vortexed into solution briefly. This mixture was warmed at 60ºC for 20 minutes to facilitate incorporation of protein into solution. This was further mixed for three hours at 37ºC on a heated shaker. After mixing, PA01 cells in TSB were diluted to a final optical density (OD) of 0.01 at 600 nm into this solution, resulting in final reagent concentrations of 40 mg mL^{-1} BSA, 200 mg mL^{-1} gelatin, and 5 mM RB in TSB. The solution was vortexed briefly to distribute the cells evenly, and then 30 μL droplets were pipetted into separate wells of a chambered coverslip (Lab-Tek, Thermo Scientific) and allowed to cool to room temperature (20ºC unless stated otherwise) to immobilize the cells. Cells were then located within the solution using an oil immersion objective (Olympus UPlanApo 100X 1.35 NA) on an inverted microscope (Zeiss Axiovert), and three dimensional (3D) protein microstructures were fabricated in a layer-by-layer fashion around individual cells according to the MPL method described in Chapter 1. Laser power (measured at the back aperture) was ~45 mW, and a step size of 0.5 μm per layer was used. Four structures were fabricated within the same well at a distance of 40 μm apart. Each microstructure was created with a nominal initial volume of ~1 pL with the potential to expand as cells grow over time. A 3D representation and a diagram illustrating the design parameters, including nominal dimensions, are shown in Figure 2.1 below.

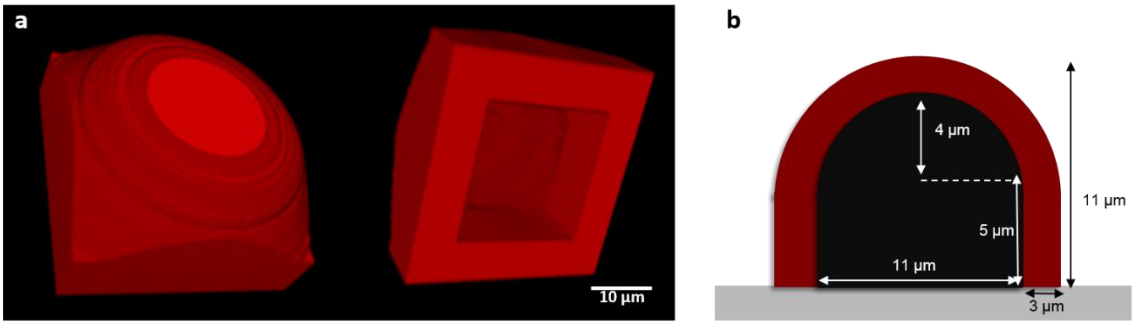

Figure 2.1 Microtrap used in antibiotic resistance studies. A three dimensional false color projection of the structure mask is shown in part (a) from above (left) and below (right). In (b) the nominal structure dimensions are diagrammed for a z-axis step size of 0.5 µm during fabrication.

Following the fabrication process, 300 µL of TSB at room temperature was introduced to each well and the entire 8-well plate was placed into a 37ºC incubator. After the temperature equilibrated, the remaining un-crosslinked gelatin solution was rinsed away using additional 37ºC TSB, leaving the cell-containing, free-standing protein microstructures adhered to the coverslip.

2.2.4 Growth Conditions and Antibiotic Dosing

Following completion of the rinsing process, cells were allowed to grow within the structures at 37ºC in an incubator with a doubling time of ~45 minutes for different lengths of time depending on the desired cell density at the time of antibiotic dosing. Cells within structures intended for high density studies were grown four hours, while those intended for low density studies were grown for 2.5 hours. This resulted in "high" density populations in which cells were ~10^{12} cells mL^{-1} and "low" density populations in which cells were $\leq 10^{8}$ cells mL^{-1} at the time of antibiotic dosing. At the respective time points, a 400 µL aliquot of 37ºC gentamicin solution was introduced into the well while simultaneously removing the solution within the well. This was achieved through the synchronized use of two pipettes and was repeated ten times in succession to ensure

accurate antibiotic concentrations within the well. Two concentrations of gentamicin in TSB were used, a minimum inhibitory concentration (MIC) of 1.6 μg/mL, and one hundred times the MIC, 160 $\mu g/mL^{-1}$, with each concentration administered to cells at both high and low densities. Controls for each parameter in which the populations were grown concurrently in structures within different wells were rinsed similarly at the respective dosing time points, with TSB only. All cells were then incubated for two hours at 37ºC. At the end of this incubation period, a 30 μM solution of propidium iodide in buffer (20 mM HEPES, 0.1 M NaCl in dH_2O, pH 7.4) was exchanged for either the TSB or antibiotic TSB solution, using the same rinsing method described above. The entirety of the culture well was incubated at room temperature for 15 minutes in aluminum foil to ensure protection from light while preparing for imaging.

2.2.5 Imaging and Data Analysis

Confocal imaging of the structures was performed at room temperature (~22ºC) using a 63X, 1.4 NA objective mounted on a confocal microscope (Zeiss LSM710) to obtain a z-step series of images using the accompanying software (Zen). Preprogrammed settings provided in the software were used for collection in the green and red channels, using the "GFP" and "propidium iodide" options, respectively. Transmission images were taken with each scan for comparison, with a total image collection time per sample of 30 minutes. Antibiotic kill rate was determined as a ratio of dead to total cells. The number of dead cells was determined by manually counting all cells stained with propidium idiode using a 3D reconstruction of the confocal scans (Zen). The total number of cells could be counted manually only for low density populations; in high-density populations, the large number of cells and tight packing prohibited using this method for discerning total cell numbers, which instead were estimated using a growth curve based on the initial cell count

and generation time. The total internal volume of the structure following expansion due to growth as determined from the cell mass boundaries was calculated from confocal reconstructions. This total structure volume was subsequently divided by the average cell volume to calculate the number of cells within a tightly packed structure of given dimensions, and this was checked against the final cell count for total cells within densely populated structures.

Each of the four parameters (high density MIC, low density MIC, High density 100X MIC, and low density 100X MIC) were tested at minimum in triplicate side by side against controls in a separate well on the same chambered coverslip.

2.3 Results and Discussion

Previous studies published by members of the Shear group have shown that population density has the ability to influence the development of antibiotic resistance in small populations of *Pseudomonas aeruginosa* [16]. The bulk of such earlier studies, however, used microstructures fabricated using BSA as the only source of protein, and were not fabricated around cells (they were, instead, used to capture motile cells). Thus, it is necessary to repeat these antibiotic resistance studies with heterogeneous solutions of protein in order to ensure that cells exhibit similar responses following growth within gelatin-containing microstructures using our new capture protocol. The following sections address the development of antibiotic resistance in small populations of cells at differing densities within BSA-gelatin structures.

2.3.1 MIC Dosing of PA01 pMRP9-1 with Gentamicin

The development of antibiotic resistance was determined by comparison of the number of cells killed versus the total cell population at different densities. Figure 2.2 displays the percentage of dead cells over the total population within microstructures at

low and high population densities following gentamicin dosing at the minimum inhibitory concentration (MIC), as well as for controls in which no antibiotic was administered.

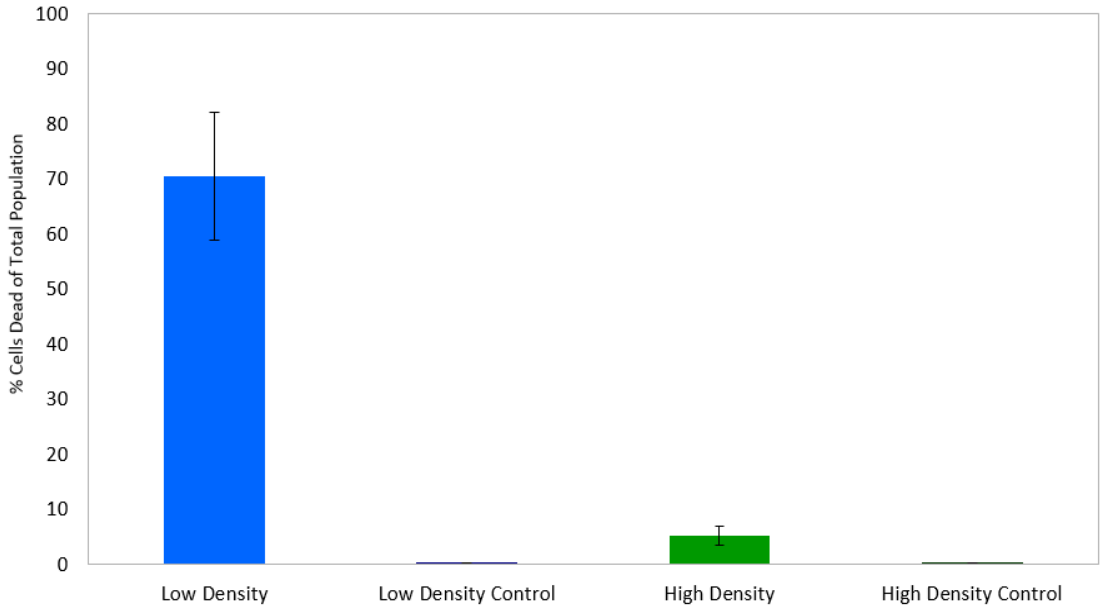

Figure 2.2 Kill rate of PA01 dosed with MIC gentamicin. Each data point represents the average percentage of dead cells to total population within individual microstructures fabricated on different days. Error bars represent pooled standard deviations for the respective parameter with $N \geq 12$. Error bars are present for the controls but cannot be viewed as a result of their small size.

The control populations, which were allowed to grow without antibiotic dosing for the duration of the experiment in adjacent wells, exhibited similar levels of cell death at both low and high density, at less than one percent. This suggests that neither the inherent properties of the structures themselves, nor the difference in population density alone, can be responsible for the differences in cell death with respect to these experiments. This supports previous observations that growing *P. aeruginosa* within BSA-gelatin microstructures does not appear to affect their survival rate as compared to free swimming populations under similar conditions, even at high population densities [17][18][33].

In stark contrast, large differences were observed in the ratio of dead cells to total population following dosing of PA01 cells with the minimum inhibitory concentration of gentamicin at the two different cell densities. The low density populations experienced a much larger response to the administration of antibiotics compared to the high density populations, with inhibited growth and increased cell death. Following the two hour dosing period, it was observed that 70 ± 12% of the low density cells were dead, as indicated by propidium iodide (PI) staining (Figure 2.3a; left). The high density populations, however, displayed much lower levels of cell death, with only 5 ± 2% of the population staining dead (Figure 2.3b; left). Previous studies performed by Shear lab members observed kill rates of 77% and 3%, respectively [16].

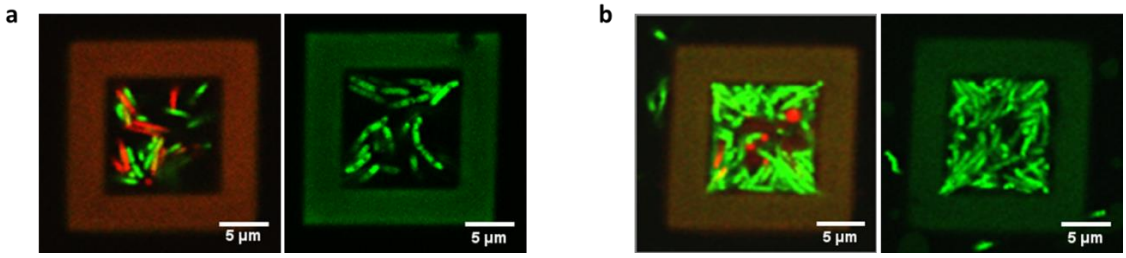

Figure 2.3 Confocal images of MIC dosed low and high density traps. False color images show dead and live cells within the structures fluorescing in the red (PI) and green (GFP) channels respectively. Differences in structure color are a result of image processing. (a) A low density population treated with gentamicin is shown (left) alongside the accompanying control population (right). (b) A high density population treated with gentamicin is shown (left) with its control (right).

2.3.2 100X MIC Dosing of PA01 pMRP9-1 with Gentamicin

A similar experiment was designed to complement the data presented in the previous section. In this subsequent experiment, cells were allowed to grow to low and high densities, and were then dosed with one hundred times the MIC. In theory, this should eliminate the majority of the cells, even those benefiting from increased resistance to

antibiotics as a result of genetic and phenotypic changes at high density. Figure 2.4 shows graphs of the mean percentage of dead cells over the total population within a structure at low and high population densities following gentamicin dosing at one hundred times the MIC, as well as for controls in which no dose was administered.

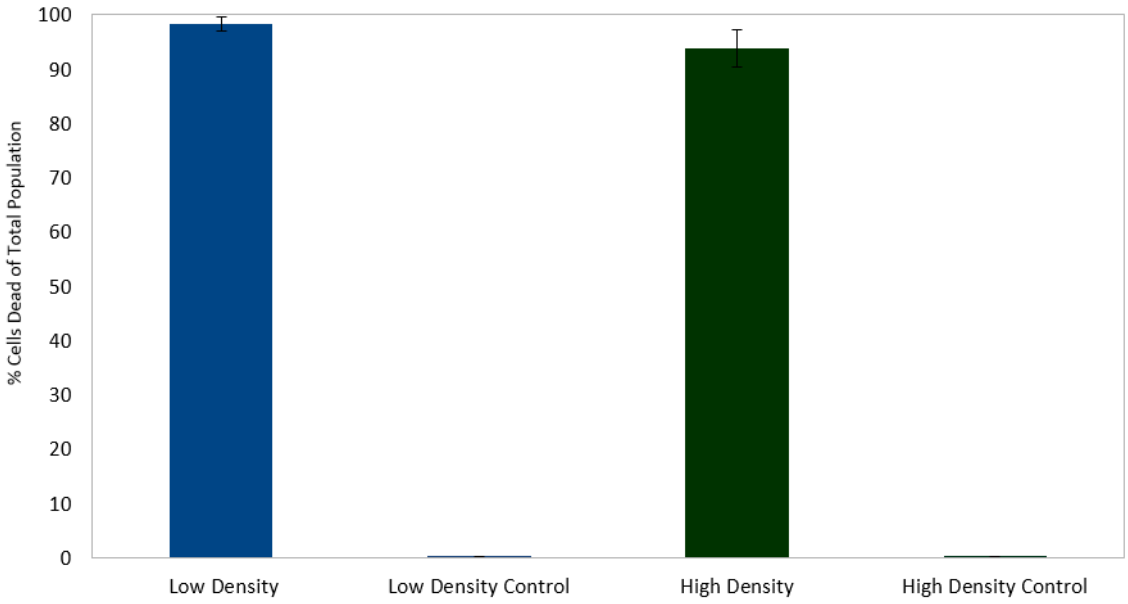

Figure 2.4 Kill rate of PA01 with 100X MIC gentamicin. Each data point represents the mean percentage of dead cells to total population within replicates of individual structures fabricated on different days. Error bars represent pooled standard deviation for the respective parameter with $N \geq 12$. Error bars are present for the controls but cannot be viewed as a result of their size.

In agreement with the data presented in the previous section, the control populations do not appear to be affected to a significant degree by either the structures themselves, or by the altered population density. Both the low and high density control populations, which were allowed to grow for the duration of the experiments in adjacent wells, experienced less than 1% cell death within the structures. This supports the previous data gathered and provides a comparison for the cells in the wells to which antibiotic was administered.

The low density structures experienced a 98 ± 2% kill rate following the dosing period (Figure 2.5a; left) while the high density structures experienced a kill rate of 94 ± 2% (Figure 2.5b; left). This high density value is similar to the 94% kill rate seen previously in studies performed by the Shear lab [16]. It appears, however, that unlike their MIC dosed counterparts, cells dosed with 100X the minimum inhibitory concentration did not see a statistical difference in kill rate between high and low density populations following the dosing process.

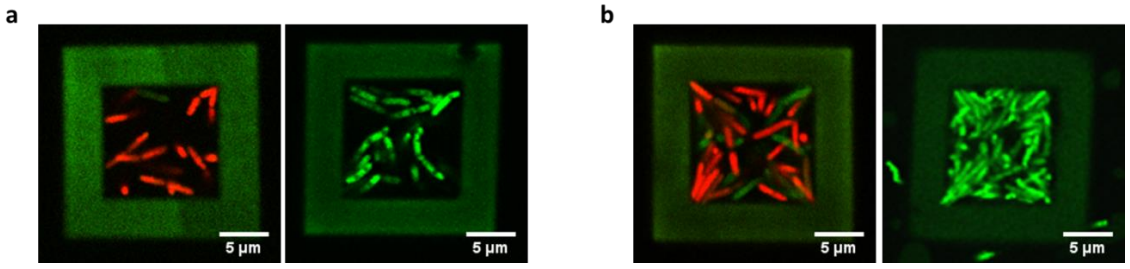

Figure 2.5 Confocal images of 100X MIC dosed low and high density traps. False color images show dead and live cells within the structures fluorescing in the red (PI) and green (GFP) channels respectively. Differences in structure color are a result of image processing. (a) A low density population treated with gentamicin is shown (left) alongside the accompanying control population (right). (b) A high density population treated with gentamicin is shown (left) with its control (right).

2.4 CONCLUSIONS

The data presented in this chapter has supported the validity of capturing/growing bacterial microcolonies within BSA-gelatin microstructures for assessing and characterizing antibiotic resistance development. All control populations were observed to behave in a manner consistent with growth in normal flask culture conditions over time [77]. The data gathered for the low and high density populations for MIC gentamicin dosing were statistically different, providing support for the concept that antibiotic resistance does begin to develop in highly dense, small aggregates. However, it was

additionally noted that at much higher concentrations of antibiotics, high cellular density does not afford protection to cells. Finally, kill rates observed in their respective categories were statistically similar to previous data gathered using BSA structures alone under similar conditions [16]. Together, this suggests that BSA-gelatin structures can be used in future resistance studies, and the data presented here may serve as a reference for future experiments.

Chapter 3: Contribution to Oxygen Depletion Studies[1]

3.1 INTRODUCTION

There are many questions still surrounding how bacterial populations regulate group behaviors such as antibiotic resistance [4][7][14]. In small populations relevant to aggregate size within chronic wound and infection sites, it has been shown that the onset of quorum sensing (QS) does not directly correlate with the development of resistance, and furthermore that resistance does appear to be density dependent at the population size investigated (~10^1 to ~10^3 cells) [16]. This leaves the mechanism of communication that facilitates the development of antibiotic resistance within a population unaccounted for [5]. In order to investigate potential means of effecting changes in genetic expression without the use of QS, the Shear and Whiteley labs collaborated to investigate levels of chemical heterogeneity within small populations of cells. In particular, it was hypothesized that local areas of oxygen depletion within a given aggregate may be, at least in part, responsible for phenotypic changes. To determine whether or not this was a possibility, a set of experiments were conducted by Whiteley lab member, Dr. Aimee Wessel, in collaboration with Talha Arshad of the Bonnecaze group and me to determine if localized pockets of oxygen depletion (<2% or 3 μM oxygen dissolved in solution) could be detected within small dense aggregates of PA01 [34][78]. Data acquisition and monitoring of the cells during the growth period was performed by Dr. Wessel, while assistance with design and fabrication of microstructures was performed by the author.

---

[1] A. K. Wessel, T. A. Arshad, M. Fitzpatrick, J. L. Connell, R. T. Bonnecaze, J. B. Shear, and M. Whiteley, "Oxygen limitation within a bacterial aggregate.," *MBio*, vol. 5, no. 2, p. e00992, Jan. 2014.
Dr. Aimee Wessel conducted plasmid transfection, imaging and data analysis. Talha Arshad developed the mathematical model predicting areas of oxygen depletion. Mignon Fitzpatrick assisted with structure design and fabricated the microstructures using μ3DP. Dr. Jodi Connell also assisted with structural design and fabrication.

3.2 EXPERIMENTAL METHODS

3.2.1 Reagents

Bovine serum albumin (BAH64-0100) was purchased from Equitech-Bio (Kerrville, TX). Rose Bengal (330000), Gelatin Type A from porcine, 300 Bloom (G-2500), and gentamicin sulfate salt (G1264) were acquired from Sigma-Aldrich (St. Louis, MO). HEPES sodium salt (AC21500-1000) was obtained from Acros Organics (Geel, Belgium). Sodium chloride (S271-3) and carbenicillin disodium salts (BP2648-1) were purchased from Fisher BioReagents (Fairlawn, NJ). Tryptic soy broth (R455052) and tryptic soy agar (1.05458.0500) were obtained from Remel Thermo Scientific (Waltham, MA) and EMD Millipore (Billerica, MA), respectively. All manufacturer recommendations for storage were followed.

3.2.2 Bacterial Strains, Plasmids and Culture Conditions

Experiments were performed using two different strains of *Pseudomonas aeruginosa* PA01 provided by the Whiteley lab. The first strain, PA01 transfected with the *gfp* plasmid pMRP9-1, served as a reference by constitutively expressing green fluorescent protein (GFP). The second, PA01 transfected with the plasmid pAW9, served as a low oxygen biosensor, by expressing GFP only in culture environments with $\leq$2% (3 μM) dissolved oxygen. Plasmid maintenance was facilitated using 150 μg mL^{-1} carbenicillin. Cultures used in the fabrication process were incubated at 37°C overnight under aerobic conditions in half-strength (0.5X) tryptic soy broth (TSB). These were subsequently diluted into fresh 0.5X TSB and vigorously aerated by shaking 5 mL cultures in 250 mL flasks at 250 rpm for a minimum of 2 hours in a 37ºC incubator before their introduction into fabrication solution. This procedure served to reduce levels of GFP that could be present in the pAW9 cultures as a result of overnight growth. Cells in culture did not exceed an

optical density (OD) of 0.8 before dilution into fabrication solution, to keep the cells in logarithmic phase.

3.2.3 Protein Hydrogel Fabrication

The fabrication precursor solution was created by sonicating Rose Bengal (RB) in 20 mM HEPES buffer (0.1 M NaCl, pH 7.4) in a 60ºC bath for one hour, then bovine serum albumin (BSA) and gelatin from porcine Type A 300 bloom (gelatin) were added and the solution was vortexed briefly. This was placed in an oven at 60ºC for 20 minutes to allow the protein to dissolve. After removal from the oven, the mixture was placed on a heated shaker for three hours at 37ºC. After mixing, PA01 cells in 0.5X TSB were diluted to a final optical density (OD) of 0.01 at 600 nm into this solution, resulting in final reagent concentrations of 25 mg mL^{-1} BSA, 200 mg mL^{-1} gelatin, and 5 mM RB in HEPES buffer. The solution was pipetted briefly to distribute the cells within solution, and then 50 µL droplets were pipetted into separate wells of a chambered coverslip (Lab-Tek, Thermo Scientific) and cooled to room temperature to solidify the gelatin solution, thus rendering the cells immobile. Cells were then located visually within solution using an oil immersion objective (Olympus PlanApo 60X 1.4 NA) on an inverted microscope (Zeiss Axiovert). Protein structures were constructed around cells within solution using the MPL technique described in Chapter 1. Laser power (measured at the objective back aperture) was ~40 mW, and a step size of 0.5 µm per layer was used. Various structures were designed throughout the course of the experiment in order to fulfill particular goals. Three-dimensional projections of structure concepts can be found in Figures 3.1 through 3.3. Structures within the same well were fabricated at opposite ends of the droplet to prevent cross-talk.

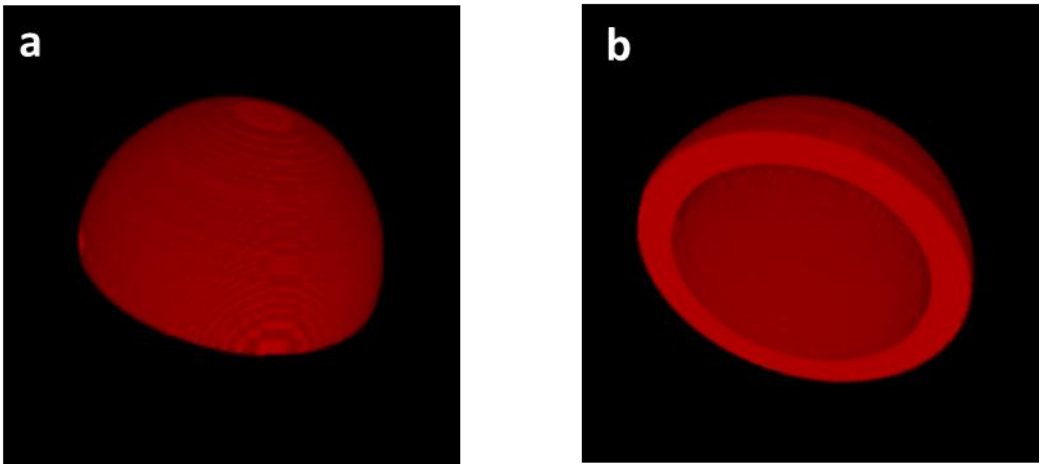

Figure 3.1 Structure designed to minimize surface area to volume ratio. This half sphere shape was designed to capitalize on the low surface area to volume ratio of spheres. Various dimensions were tested with respect to internal diameter and wall thickness. (a) A view of the outside of the dome. (b) A view of the hollow interior.

The shape illustrated in Figure 3.1 is the primary structure design used in these studies, and underwent extensive modification throughout the experimental process. Initially, these half spheres, or "domes," were created to have internal volumes of 2 pL (18 μm inner base diameter) and 9 pL (32 μm inner base diameter), respectively. Both the 2 pL and 9 pL structures were tested with wall thicknesses of 4 μm and 8 μm, for a total of four potential designs. The majority of the data presented here involve structures with these starting dimensions. Later, domes of even greater volume were created with volumes of 24 and 50 pL, respectively, which also featured 8 μm walls, but they are not covered here.

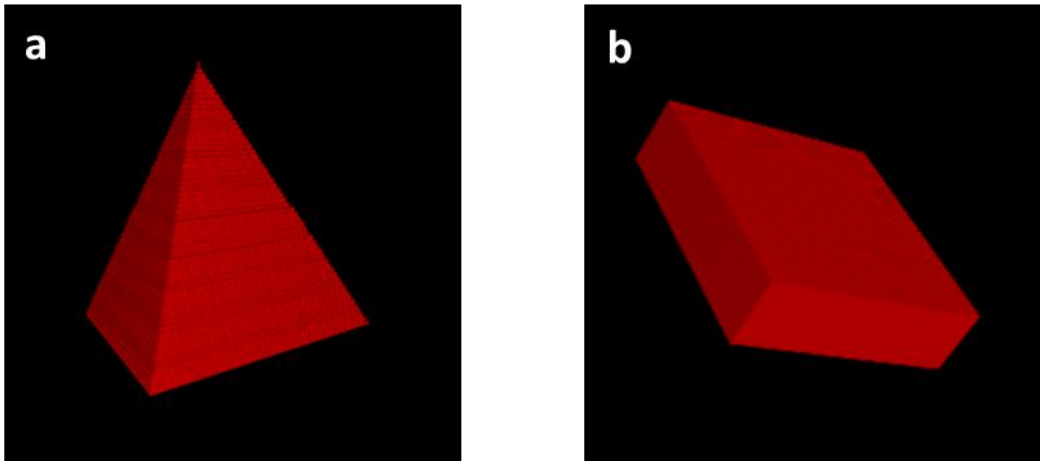

Figure 3.2 Structural designs maximizing surface area to volume ratio. (a) A hollow pyramidal design. (b) A hollow short rectangular design.

Figure 3.2 presents two structures that were designed with the intention of prohibiting localized oxygen depletion. It was assumed that their higher surface area to volume ratio would be of benefit in this endeavor, but the flexible gelatin walls enabled stretching that eventually contorted both shapes such that they began to resemble domes themselves.

The structure that eventually proved most useful in reducing oxygen depletion was a dome replica raised above the surface of the glass by means of structural supports, or stilts, made of the same material. This structure is presented in Figure 3.3 below. This design featured an internal volume of 9 pL (32 μm inner base diameter) with 8 μm walls, and served as a comparison for dome structures on the surface of the coverslip.

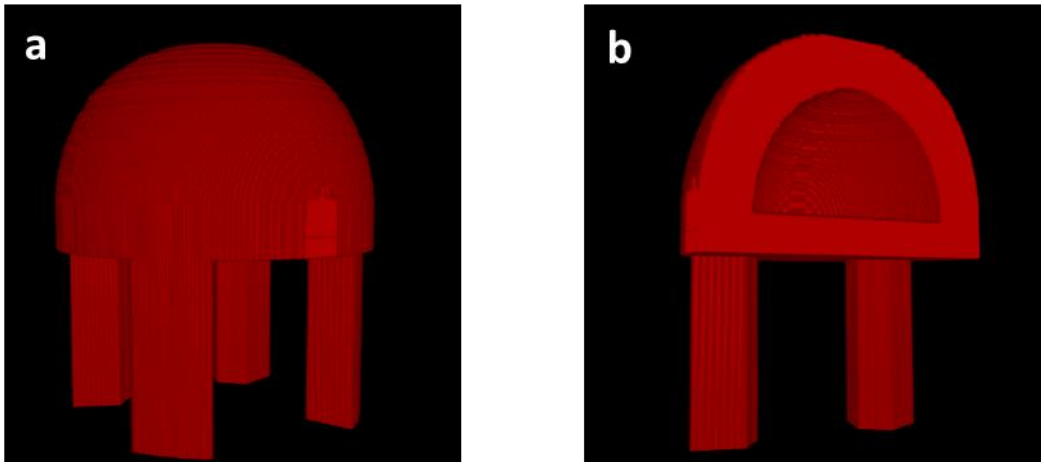

Figure 3.3 Structure designed to remove glass diffusion barrier. This design mimics the half sphere shape described previously, but with the added benefit of stilts, such that the entire half sphere structure is removed from contact with the glass. (a) The exterior of the design. (b) A view of the hollow interior.

Upon completion of fabrication of microstructures around one or more bacterial cell, the multi-well plate was warmed to 37ºC in an incubator to soften the gelatin droplet, and then 37ºC TSB was used to rinse away any solution that had not been crosslinked. The residual structures containing their respective cell types were then analyzed.

3.2.4 Imaging and Data Analysis

Following the fabrication process, cells were allowed to grow in a microscope incubator (InVivo Scientific) at 37°C for up to 7 hours, depending on the experimental parameters. During this time they were observed periodically via light microscopy (Nikon TS100). Following this growth period, cells were removed from the incubator and imaged at ~25°C using a 63X, 1.4 NA objective mounted on a confocal microscope (Leica) to obtain a z-step series of images in the green and red channels. These channels were configured with a 488-nm excitation with emission centered at 515 nm (35-nm slit width) for green, and a 543-nm excitation with emission centered at 640 nm (120-nm slit width)

for red. Imaging was performed periodically over a 9 hour period after the cells were removed from the incubator.

Trap dimensions, cell population volumes and the total voxels of GFP from constitutively expressing PA01 pMRP9-1 and PA01 pAW9, respectively, were quantified with Imaris software (Bitplane AG). Isosurface mode of the Surpass module was used to generate isosurfaces of the red channel stacks, and these were used to calculate the internal volume of the structures at various time points [34].

3.3 Results and Discussion

3.3.1 Cell Growth at Maximum Density

Prior to examining the potential for zones of oxygen depletion to arise within these microstructures, experiments were performed using PA01 pMRP9-1. This allowed for observation of cell growth rate within the traps as indicated by the production of GFP. Both the 2 pL (18 μm inner base diameter) and 9 pL (32 μm inner base diameter) half sphere designs with 8 μm walls were tested, and Figure 3.4 displays the cell growth within the latter over a period of 8-15 hours following the fabrication process. In this figure, it can be seen that the traps reached maximal densities of ~10^{11} to ~10^{12} cells mL^{-1} within the structure between hours 8 and 11, but continued to grow and divide after this point. By hour 15, the growing population of cells had stretched the walls of the trap such that the inner diameter at its largest point was closer to ~55 μm. This result illustrates that populations of cells can continue to increase within a structure, despite having reached densities higher than those witnessed in flask culture where cells tend to enter the stationary phase at densities ≥10^{8} cells mL^{-1} [79]. In addition, these observations became key in subsequent experiments to determine the population size required for oxygen depletion to occur.

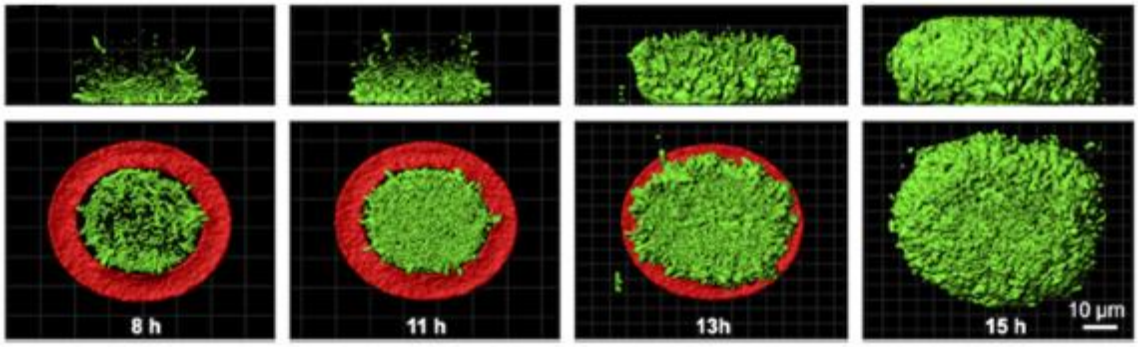

Figure 3.4 Confocal images of PA01 strain pMRP9-1 growth over time. The top row provides a 3D reconstruction side view of the confocal z-stack and the bottom row is a top down view of the same. Cells are designated in green while an isosurface of the base of the structure is shown in red. Structure walls are not included for clarity [34].

3.3.2 Population Increase and Oxygen Depletion

The half sphere traps were then used to determine the population size necessary for the formation of oxygen depletion zones within an aggregate. In these studies, PA01 pAW9 was used and the production of GFP served as an indicator of low oxygen levels (<2%) [80]. Cells exhibited no detectable fluorescence until the population increased to a point where oxygen concentration within the aggregate dropped below 2% (3 µM) at which time the GFP reporter became active. Figure 3.5 illustrates this process occurring within a dome structure with an initial internal volume of 9 pL. The time points shown occur after cells have reached a maximum density of ~10^{11} to ~10^{12} cells mL^{-1} and the structure is full. It can be seen in the top row that the cells continued to grow as the structure stretched, as visualized by the increasing size of the blue population volume isoform and distension of the red structure walls. The bottom row contains identical images with the isoforms removed to enable visualization of GFP expression from the reporter. It can be seen that despite reaching their maximum density, the cells do not begin expressing GFP until the

population volume has increased to nearly 55 pL, with a radius of approximately 27 μm. This was repeated with a 2 pL trap which reached a final volume of 9 pL and a radius of 16 μm at the same time point, but the reporter was never activated. If left to grow longer, the structures eventually burst with no GFP detected.

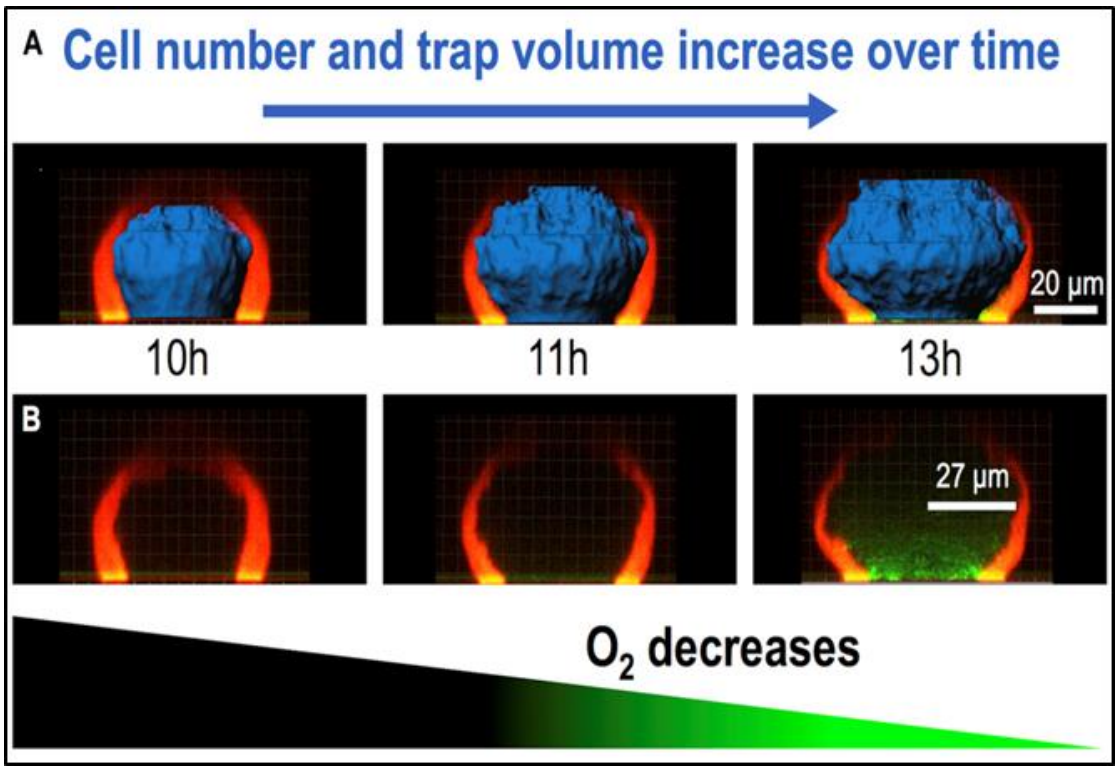

Figure 3.5 Confocal images of PA01 strain pAW9 over time. The top and bottom row were created from the same confocal scans from left to right with structure fluorescence indicated in red. In (A), an isoform reconstruction of the total cell population is shown in blue to aid in visualization. In (B), cells isoforms are not shown to enable visualization as the low oxygen reporter begins to express GFP, as indicated by the appearance of green GFP fluorescence [34].

Microstructure dimensions required to activate the low oxygen reporter were investigated further using a comparison of different types of structures. Figure 3.6 demonstrates that despite having maximal densities and continued population size increase,

some surface adhered structures still did not develop low oxygen regions. The first data point of the plot in Figure 3.6A (and confocal data in Figure 3.6B) shows that the 2 pL structure, which stretched to a volume of 9 pL with a 16 μm radius, did not show activation of the reporter. The second data point illustrates the 9 pL structure which stretched to a volume of approximately 55 pL with a radius of ~27 μm (Figure 3.6A), and as before, the reporter is activated (Figure 3.6B). However, the third point illustrates what happens when the oxygen diffusion barrier is removed by separating the structure from the coverslip (Figure 3.6C). In this case, oxygen is free to diffuse through the bottom of the structure, and the low oxygen reporter strain does not begin to produce GFP (Figure 3.6B).

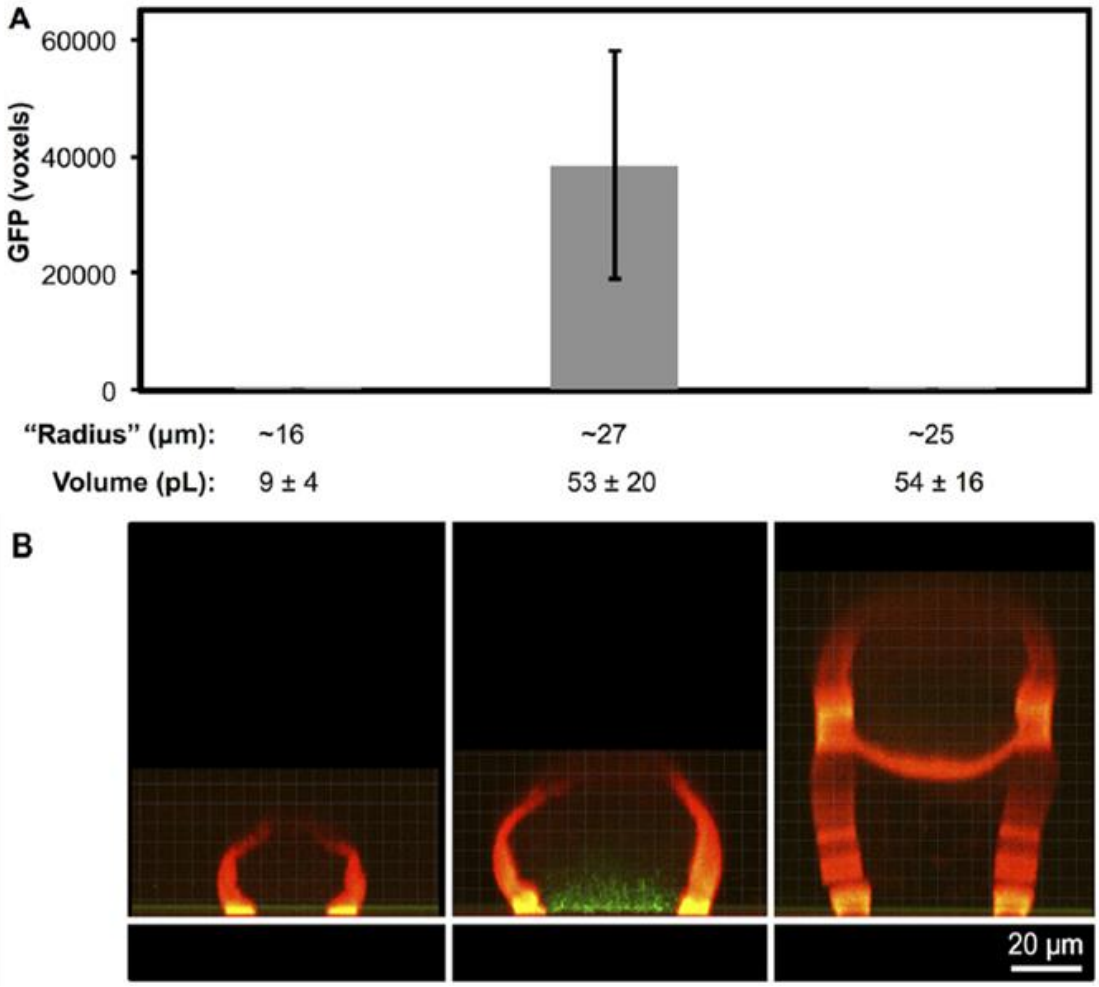

Figure 3.6 Plot of GFP signal from PA01 strain pAW9 in surfaced adhered and raised structures with accompanying confocal images. Both the plot and the images represent final time points at which the structures have stretched to the given dimensions. In (A) GFP voxels per structure are shown, with structure radii (estimated from the widest part of the structure) and volumes (calculated from an isoform) indicated below each data point. (B) corresponding confocal images in which the cells are present but imperceptible unless expressing GFP as seen in the middle panel in green, structures are in red [34].

Finally, an experiment was performed to confirm that despite the removal of the oxygen diffusion barrier represented by the coverslip, oxygen depletion could occur provided the aggregate achieved a much larger population size (Figure 3.7). It is clear that

despite being raised from the coverslip, at 95,000 cells the reporter strain begins to produce GFP, indicating low levels of oxygen. In addition, mathematical models were generated (COMSOL Multiphysics Engineering Simulation Software v 3.5a) using various structure radii and modeled upon oxygen reaction rates within the structure by PA01 where it was determined that the data correlated with the predicted structural dimensions for oxygen depletion [34].

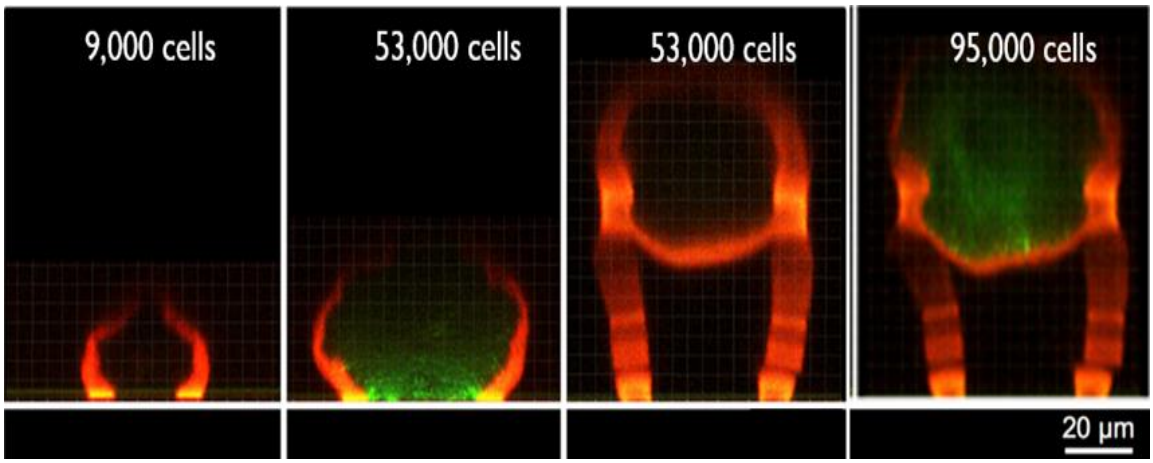

Figure 3.7 Confocal images of PA01 strain pAW9 demonstrating expression of low-oxygen GFP reporter. The surface-adherent cells begin to exhibit fluorescence upon reaching a population size of 53,000 cells (left two panels), whereas cells in a raised structure must attain a population size of 93,000 cells before exhibiting fluorescence (right two panels). In all four panels the structures can be seen in red, however only in panels two and four can cells be distinguished as a result of activation of the GFP reporter shown in green [34].

The cell populations described in this chapter did not begin to experience regions of oxygen depletion until they had reached approximately 53,000 cells at maximal density. While this does provide evidence of chemical heterogeneity within the population, it does not support the hypothesis that this depletion plays a role in antibiotic resistance. Previous studies performed in the Shear lab indicate that a dense population of as few as ~150 cells

can begin to develop antibiotic resistance, two orders of magnitude fewer than the number shown by these studies to produce low oxygen regions within an aggregate [16].

3.4 CONCLUSIONS

Determination of chemical gradients within small bacterial populations can provide important information about mechanisms of effecting population-wide genetic changes [25][81][82]. Development of oxygen depletion regions within organized pockets of cells may have the potential to induce these changes as a result of cell stress. The studies reported in this chapter demonstrate that surface adhered cellular aggregates at maximal density (~10^{12}) are required to reach a critical size of ~55 pL with a radius of ~27 μm in order to develop low oxygen regions in which the concentration of extracellular oxygen dips below 2% or 3 μM. This was observed at a population size of approximately 10^4 cells. As a result, while this heterogeneity may induce cellular changes in genetic expression, it does not appear to be responsible for the development of antibiotic resistance, which can occur in a population of as few as ~10^2 cells.

In addition to illustrating the conditions necessary for the development of low oxygen regions, it was also shown that removal of the oxygen diffusion barrier presented by the glass can alter the required dimensions for this type of oxygen depletion to occur. Furthermore, the data correlated with a constructed mathematical model that may enable prediction of low oxygen pockets within microbial communities [34]. The results of this set of experiments also serve to highlight the capabilities of three dimensional protein microstructures in providing well-defined cell culture environments for population sizes and densities relevant to spread and growth of *in vivo* infections.

Chapter 4: Cell Surface Attachment and Removal

4.1 Introduction

In addition to seeking knowledge regarding the way bacteria communicate and influence genetic expression within a population, it is also important to learn how to inhibit the formation of these small dense populations in order to disrupt communication and prevent the development of unwanted phenotypes [35][36][83][84]. Many studies have tested the effectiveness of surface-immobilized antimicrobials such as silver ions, as wells as surface polymer coatings containing antibiotics for slow release [85][86]. In addition, antifouling coatings have been investigated as a means to prohibit attachment [87]. Another common method is the three-dimensional patterning of surfaces in order to reduce contact angle and discourage cells from attaching upon contact [88][89]. Three dimensionally printed microstructures also offer a convenient, easily manipulated means of designing and efficiently testing various surfaces for limiting bacterial growth. The goal of the experimental designs presented in this chapter is to inhibit cell attachment while encouraging cell sequestration from the general population in an attempt to lower the amount of cells capable of initiating aggregates and participating in the infection process. Cells collected in this manner could potentially be later removed from solution or occupy a temporary reservoir within a disposable device.

4.2 Experimental Methods

4.2.1 Reagents

Rose Bengal (330000) was purchased from Sigma-Aldrich (St. Louis, MO). Bovine serum albumin (BAH64-0100) and Gelatin Type A from porcine, 60 Bloom (16560) were obtained from Equitech-Bio (Kerrville, TX), and Electron Microscopy Sciences (Hatfield, PA), respectively. HEPES sodium salt (AC21500-1000) was acquired from Acros

Organics (Geel, Belgium). Sodium chloride (S271-3) was obtained from Fisher BioReagents (Fairlawn, NJ). Tryptic soy broth (R455052) and tryptic soy agar (1.05458.0500) were purchased from Remel Thermo Scientific (Waltham, MA) and EMD Millipore (Billerica, MA), respectively. Glutaraldehyde (18426) was acquired from Ted Pella, Inc (Redding, CA). All manufacturer recommendations for storage were followed.

4.2.2 Bacterial Strains, Plasmids and Culture Conditions

Gfp-expressing *Pseudomonas aeruginosa* PA01 pMRP9-1 provided by the Whiteley lab was used for all experiments. Cultures were grown on plates of tryptic soy agar (TSA) with 100 μg mL^{-1} carbenicillin for plasmid maintenance. Cells were started from a plate and incubated in tryptic soy broth (TSB) under aerobic conditions at 37°C overnight. The following day, cells were diluted and grown to mid-logarithmic phase in fresh TSB. Following the fabrication of structures, these cells were diluted to an optical density (OD) of 0.01 at 600 nm and deposited into the wells.

4.2.3 Protein Hydrogel Fabrication

A hydrogel fabrication solution was created using TSB containing 40 mg mL^{-1} bovine serum albumin (BSA), 200 mg mL^{-1} gelatin from porcine Type A 60 bloom, and 5 mM Rose Bengal (RB). As discussed previously, RB was first sonicated into TSB at 60ºC for one hour, followed by the addition of the protein to solution, whereupon the mixture was briefly vortexed and incubated at 60ºC for twenty minutes. This solution was further mixed on a heated shaker at 37ºC for 3 hours before dilution to the final volume with TSB, which was similarly briefly vortexed. 30 μL aliquots of this solution were administered into separate wells of a chambered coverslip (Lab-Tek, Thermo Scientific). Using an oil immersion objective (Olympus UPlanApo 100X, 1.35 NA) on an inverted microscope (Zeiss Axiovert), free-standing 3D protein microstructures were created using

the MPL method described in Chapter 1. However, due to a decrease in step size from 0.5 µm per layer to 0.25 µm per layer resulting in more scans per micron axially, it was necessary to lower the incident laser power. Thus, power at the back aperture for these experiments was adjusted to ~35 mW. Individual structures within the same well were fabricated separated by a distance of 10 µm. Each microstructure featured a two-by-two array of pyramidal funnels, with each cone containing its own respective collection chamber beneath. Each collection chamber was designed to have an initial volume of ~4 pL with the potential to expand over time. Four designs were compared against one another simultaneously within the same well, and each design was replicated four times, providing a total of 16 two-by-two arrays per well. 3D representations and diagrams illustrating design parameters for the quadrants, including nominal dimensions for a fabrication step size of 0.25 µm, are shown in Figures 4.1 - 4.4 below.

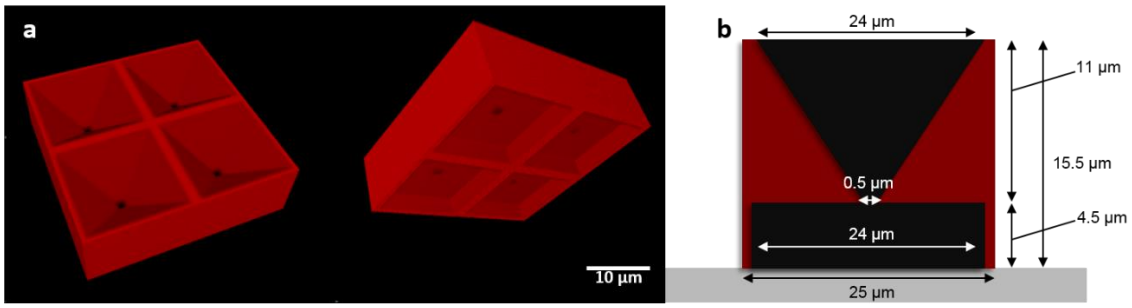

Figure 4.1 Microtrap used in attachment studies with a 0.5 µm aperture. The aperture is approximately one cell width across. A three dimensional projection of the structure mask layers is shown in part (a) from above (left) and below (right). (b) The nominal structure dimensions.

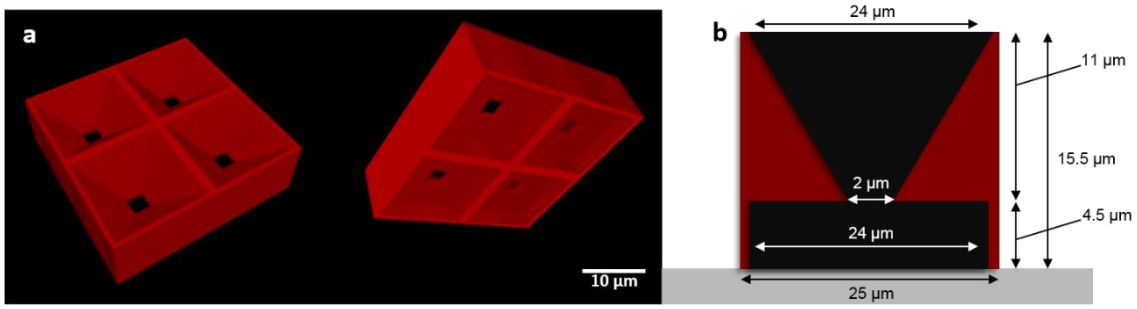

Figure 4.2 Microtrap used in attachment studies with a 2 µm aperture. The aperture is approximately one cell length across. A 3D projection of the structure mask layers is shown in part (a) from above (left) and below (right). (b) The nominal structure dimensions.

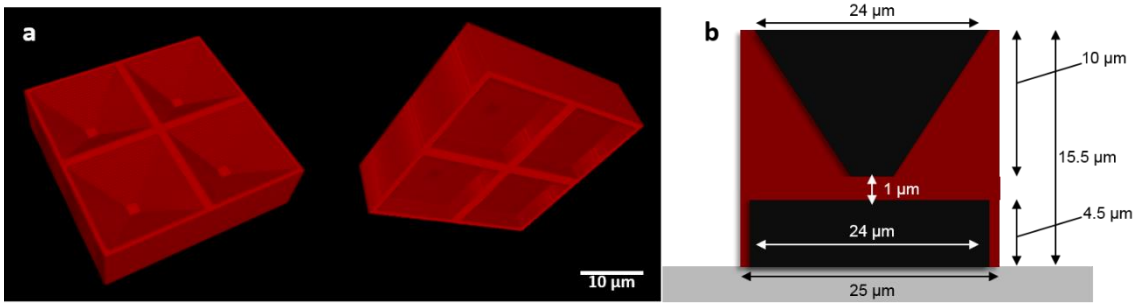

Figure 4.3 Microtrap used in attachment studies with a closed (ie., no) aperture. Layers partition the funnel from the collection chamber, preventing cells from entering. A 3D projection of the structure mask layers is shown in part (a) from above (left) and below (right). (b) The nominal structure dimensions.

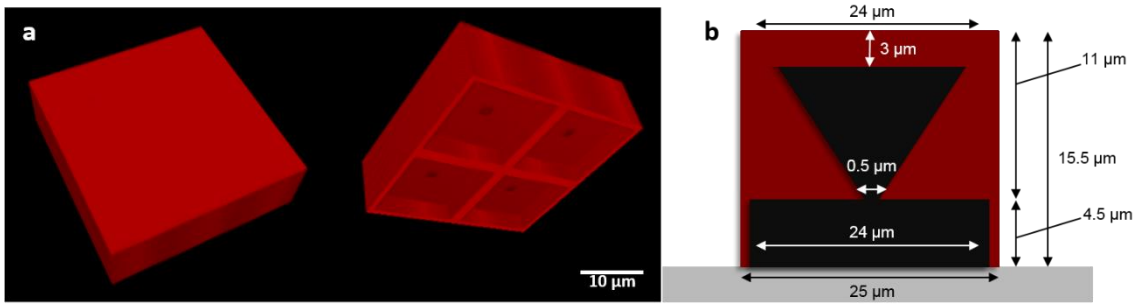

Figure 4.4 Microtrap used in attachment studies with a flat top. Layers cover the funnel completely at the top, preventing cells from entering either section below. A 3D projection of the structure mask layers is shown in part (a) from above (left) and below (right). (b) The nominal structure dimensions.

Upon completion of the structures, 300 μL of room temperature (20ºC unless otherwise indicated) TSB was administered to each well and the multi-well plate was placed into a 37ºC incubator. Following temperature equilibration, the melted hydrogel solution was rinsed away using additional 37ºC TSB, leaving behind free-standing 3D protein microstructures.

4.2.4 Cell Growth Conditions

Immediately following the removal of excess hydrogel solution and the TSB rinse, cells were added to the wells at an OD of 0.01 at 600 nm. This cell solution was pipetted up and down five times to mimic flow conditions, encourage even cell distribution, and enable a portion of the cells to fall upon the structures from above. The chambered coverslips were then left at room temperature for 20 hours, undisturbed, and covered to prevent light exposure. Following this growth period, each well was rinsed thrice gently with room temperature TSB before imaging.

4.2.5 Imaging and Data Analysis

All imaging was performed on an inverted microscope (Zeiss Axiovert) with an oil immersion lens (Olympus UPlanApo 100X 1.35 NA). Cells attached to the funnel portion of the structure were counted by sight at the time of imaging. Cells within the collection chambers were counted in a similar manner at the time of imaging, then all cells were killed by a 15 minute incubation in a room temperature solution containing 5.0% glutaraldehyde in buffer (20 mM HEPES, 0.1 M NaCl in dH_20, pH 7.4) and counted again. All measurements were performed in triplicate. One final measurement was performed in which the inoculation density was increased to an OD of 0.1 at 600 nm.

4.3 Results and Discussion

In the following sections, data is presented as manual cell counts of attachment to the top, funnel portion of the structure versus cells present in the chamber below. The initial design presented in Figure 4.1, and adjusted slightly in 4.2, was created with the intention of limiting bacterial surface attachment while providing a collection receptacle to remove cells from the solution either permanently or temporarily. The designs illustrated in Figure 4.3 and Figure 4.4 prohibit cells from entering the chamber, and are meant to serve as controls. Consequently, their chamber populations are represented by cell counts of zero.

4.3.1 Low Density Inoculation

The majority of the structures were inoculated with a population of 0.01 OD at 600 nm, as previously stated. The cells were introduced using a pipette, and thoroughly dispersed in solution by pipette mixing. This resulted in a number of cells coming to rest on top of the structures, in addition to the cells that encountered the tops of the structures through swimming motility. Following the undisturbed overnight growth period, cells had formed aggregates atop the structures and on the surrounding coverslip. The rinse served to eliminate the aggregates leaving only the tightly bound, well-adhered cells remaining attached to the funnel portions of the structures. Free swimming cells remained within the chambers below, but the apertures remained open, enabling cells to potentially exit the structures. A representative illustration of cell attachment and collection for the arrays containing the 0.5 μm aperture is presented in Figure 4.5.

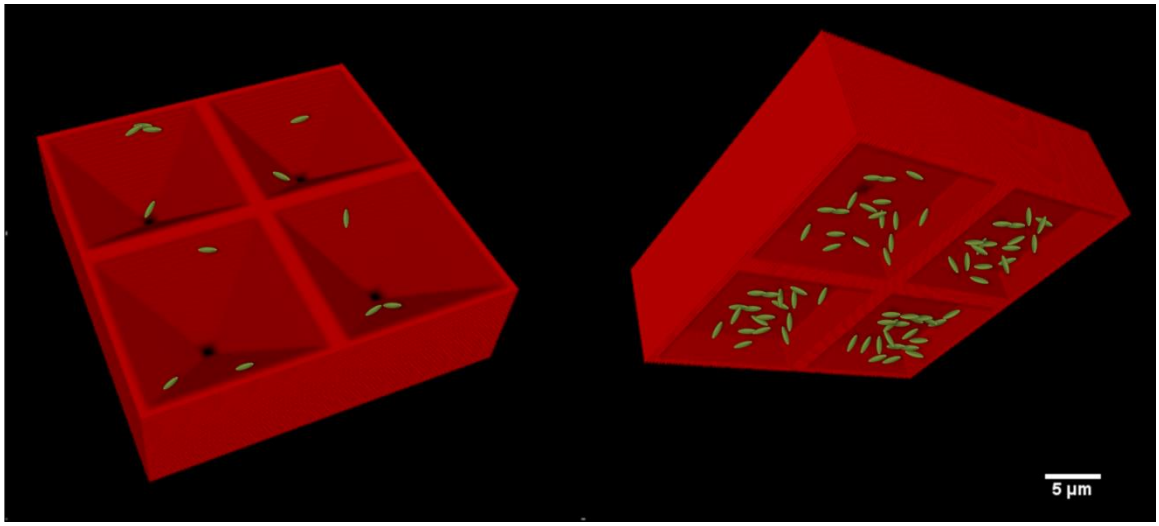

Figure 4.5 Graphic representation of cell organization in attachment studies. Relative cell dimensions are illustrated approximately to scale. Cells are shown as green upon the red background of the array viewed from above (left) and below (right). The structure displayed is modeled after the arrays containing the 0.5 µm apertures.

Cells were counted in each quadrant using the method described in previous sections, and data for all quadrants for each set of conditions were averaged to provide the overall data shown in Figure 4.6. As discussed earlier, cells were denied access to the bottom chambers in the closed aperture and flat top structures modeled in Figures 4.3 and 4.4, resulting in a value of zero for those data points on the graph.

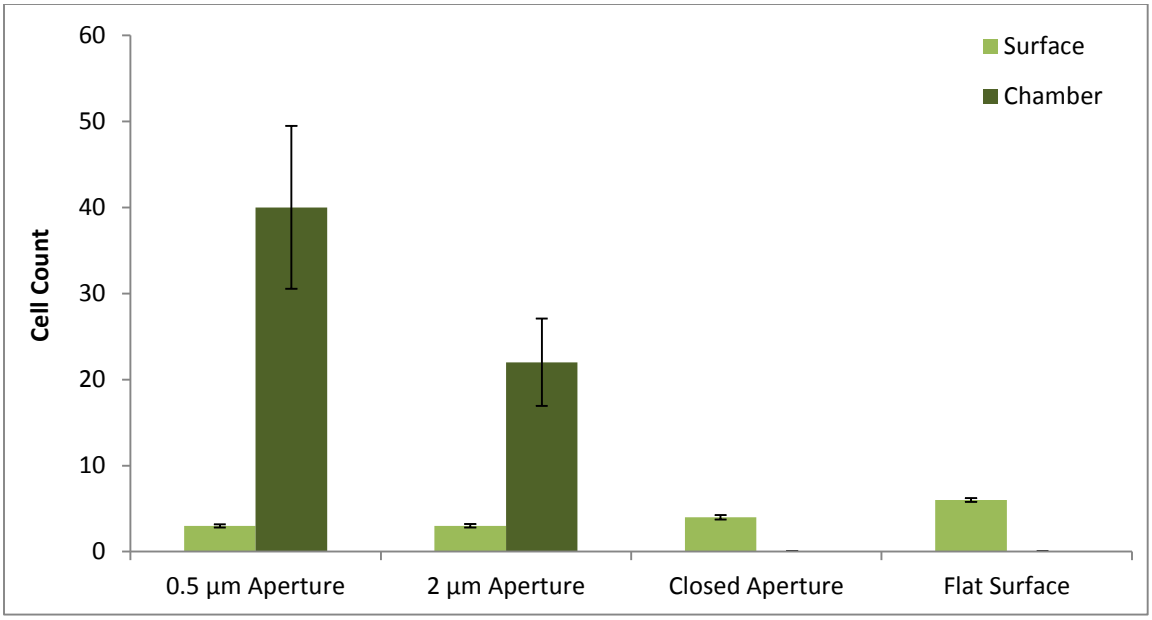

Figure 4.6 Mean number of cells observed per quadrant in attachment studies. Each data point represents replicates over multiple days, with error bars calculated by pooled standard deviation for each parameter ($N \geq 16$). Chamber values for Closed Aperture and Flat Surface are zero.

Average cell surface attachment for the two open aperture arrays was statistically the same. Each had a mean of 3 cells attached per quadrant with a standard deviation of less than 1 cell. The two controls, however, were both statistically different from results for the two experimental structures and from each other. The array with closed apertures had a mean attachment of 4 cells per quadrant while the flat surface array had 6, with standard deviations well under 1 cell.

The chamber counts for the arrays with the 0.5 µm and 2 µm apertures did differ significantly from one another. Higher numbers of cells were consistently observed in the chambers with the smaller aperture, at an average of 40 ± 9 cells, versus the chambers with the larger aperture, which had an average of 22 ± 5 cells.

Despite the difference in aperture size for the two test arrays, the level of surface attachment was the same. It is possible that the tapering effect of the funnel walls was

effective in directing cells downwards into the collection chamber regardless of the aperture size, provided cells were able to fit through the opening. Since the smaller of the two apertures was designed to be approximately the width of the average cell, this would enable most cells entrance to the bottom portion of the structure. Conversely, the size of the opening may have had a greater effect on the ability to retain the cells within the chamber, since the larger of the two apertures was designed to be approximately one cell length. This may have resulted in the large difference between cell counts for the collection chambers. This tapering effect has been shown to occur by the Shear lab in previous studies, where cells were directed through a small aperture that provided more facile entry than exit, effectively trapping the cells inside [16][76]. This could also offer an explanation for the higher level of surface attachment in the closed aperture array, where cells would be directed by this effect but not collected and removed, potentially enabling more opportunities for the cells to encounter the surface area. However, this would not necessarily explain the higher levels of attachment on the flat surface control, which has a lower overall surface area available for contact and attachment. This difference may be an artifact of the rinsing process, and further experiments must be conducted to determine if this is the case.

4.3.2 High Density Inoculation

A repeat experiment was performed using the same four structure designs, but inoculating with an initial cell density of 0.1 OD at 600 nm, an order of magnitude greater than that of the previous experiments. It was noted that upon rinsing however, this change in inoculation density did not seem to make a significant difference, and thus the concept was abandoned.

4.4 CONCLUSIONS

The information presented in this chapter suggests a potential technique that can be used for inhibiting bacterial surface attachment as well as removing cells from the general population within a fluid environment. This could be applied as a means to reduce fouling in flow-based systems, in which the walls of a channel could be patterned in such a way as to inhibit attachment and direct cells out of the bulk flow. The implications of inhibiting cell attachment are key in prohibiting the formation of biofilms as a result of cellular communication within a population [88]. Furthermore, inhibiting biofilm development has the potential to help lower the ability of cells to develop increased virulence, pathogenicity, and antibiotic resistance [22][26].

According to the data presented, the funnel and collection chamber do appear to have an effect on cell surface attachment. While the aperture size did not affect the number of cells adhered to the funnel walls, it did have an effect on cell retention in the collection chamber, with the larger aperture resulting in a lower chamber count. Further optimization is necessary to determine the best funnel pitch and aperture size to achieve minimal surface attachment and high collection efficiency. In addition, other designs may provide the opportunity to facilitate cell recycling into the fluid environment while maintaining low surface attachment. Finally, to elucidate whether or not the higher surface attachment on the flat surface is an artifact, it may be necessary to perform aggregate counts before rinsing the structures for final cell attachment counts. Alternatively, incubating the cells at 37ºC and imaging throughout the duration of the experiment may provide information that cannot be discerned under the conditions presented in this study.

References

[1] J. M. Henke and B. L. Bassler, “Bacterial social engagements.,” *Trends Cell Biol.*, vol. 14, no. 11, pp. 648–56, Nov. 2004.

[2] M. R. Parsek and E. P. Greenberg, “Sociomicrobiology: the connections between quorum sensing and biofilms.,” *Trends Microbiol.*, vol. 13, no. 1, pp. 27–33, Jan. 2005.

[3] B. L. Bassler and R. Losick, “Bacterially speaking.,” *Cell*, vol. 125, no. 2, pp. 237–46, Apr. 2006.

[4] G. B. Rogers, L. R. Hoffman, M. Whiteley, T. W. V Daniels, M. P. Carroll, and K. D. Bruce, “Revealing the dynamics of polymicrobial infections: implications for antibiotic therapy.,” *Trends Microbiol.*, vol. 18, no. 8, pp. 357–64, Aug. 2010.

[5] A. M. Stevens, M. Schuster, and K. P. Rumbaugh, “Working together for the common good: cell-cell communication in bacteria.,” *J. Bacteriol.*, vol. 194, no. 9, pp. 2131–41, May 2012.

[6] K. H. Turner, J. Everett, U. Trivedi, K. P. Rumbaugh, and M. Whiteley, “Requirements for Pseudomonas aeruginosa acute burn and chronic surgical wound infection.,” *PLoS Genet.*, vol. 10, no. 7, p. e1004518, Jul. 2014.

[7] S. L. Gellatly and R. E. W. Hancock, “Pseudomonas aeruginosa: new insights into pathogenesis and host defenses.,” *Pathog. Dis.*, vol. 67, no. 3, pp. 159–73, Apr. 2013.

[8] S. Häussler and T. Becker, “The pseudomonas quinolone signal (PQS) balances life and death in Pseudomonas aeruginosa populations.,” *PLoS Pathog.*, vol. 4, no. 9, p. e1000166, Jan. 2008.

[9] J. M. Willey, L. M. Sherwood, and C. J. Woolverton, *Prescott’s Microbiology*, 9th ed. New York, NY: McGraw-Hill Education, 2013.

[10] H. Cho, H. Jönsson, K. Campbell, P. Melke, J. W. Williams, B. Jedynak, A. M. Stevens, A. Groisman, and A. Levchenko, “Self-organization in high-density bacterial colonies: efficient crowd control.,” *PLoS Biol.*, vol. 5, no. 11, p. e302, Oct. 2007.

[11] H. J. Kim, J. Q. Boedicker, J. W. Choi, and R. F. Ismagilov, “Defined spatial structure stabilizes a synthetic multispecies bacterial community.,” *Proc. Natl. Acad. Sci. U. S. A.*, vol. 105, no. 47, pp. 18188–93, Nov. 2008.

[12] S. Wuertz, S. Okabe, and M. Hausner, “Microbial communities and their interactions in biofilm systems: an overview.,” *Water Sci. Technol.*, vol. 49, no. 11–12, pp. 327–36, Jan. 2004.

[13] T. Bjarnsholt, M. Alhede, M. Alhede, S. R. Eickhardt-Sørensen, C. Moser, M. Kühl, P. Ø. Jensen, and N. Høiby, “The in vivo biofilm.,” *Trends Microbiol.*, vol. 21, no. 9, pp. 466–74, Sep. 2013.

[14] A. K. Wessel, L. Hmelo, M. R. Parsek, and M. Whiteley, “Going local: technologies for exploring bacterial microenvironments.,” *Nat. Rev. Microbiol.*, vol. 11, no. 5, pp. 337–48, May 2013.

[15] B. Kaehr and J. B. Shear, “Mask-directed multiphoton lithography.,” *J. Am. Chem. Soc.*, vol. 129, no. 7, pp. 1904–5, Feb. 2007.

[16] J. L. Connell, A. K. Wessel, M. R. Parsek, A. D. Ellington, M. Whiteley, and J. B. Shear, “Probing prokaryotic social behaviors with bacterial ‘lobster traps’.,” *MBio*, vol. 1, no. 4, pp. e00202–10–, Jan. 2010.

[17] J. L. Connell, E. T. Ritschdorff, M. Whiteley, and J. B. Shear, “3D printing of microscopic bacterial communities.,” *Proc. Natl. Acad. Sci. U. S. A.*, vol. 110, no. 46, pp. 18380–5, 2013.

[18] J. Kim, J. L. Connell, M. Whiteley, and A. J. Bard, “Development of a versatile in vitro platform for studying biological systems using micro-3D printing and scanning electrochemical microscopy.,” *Anal. Chem.*, vol. 86, no. 24, pp. 12327–33, Dec. 2014.

[19] J. L. Connell, J. Kim, J. B. Shear, A. J. Bard, and M. Whiteley, “Real-time monitoring of quorum sensing in 3D-printed bacterial aggregates using scanning electrochemical microscopy.,” *Proc. Natl. Acad. Sci. U. S. A.*, vol. 111, no. 51, pp. 18255–60, Dec. 2014.

[20] J. Duay, J. Elliott, J. B. Shear, and K. J. Stevenson, “Transparent Carbon Ultramicroelectrode Arrays: Figures of Merit for Quantitative Spectroelectrochemistry for Biogenic Analysis of Reactive Oxygen Species.,” *Anal. Chem.*, vol. 87, no. 19, pp. 10109–16, Oct. 2015.

[21] O. Rendueles and J.-M. Ghigo, “Multi-species biofilms: how to avoid unfriendly neighbors.,” *FEMS Microbiol. Rev.*, vol. 36, no. 5, pp. 972–89, Sep. 2012.

[22] S. T. Rutherford and B. L. Bassler, “Bacterial quorum sensing: its role in virulence and possibilities for its control.,” *Cold Spring Harb. Perspect. Med.*, vol. 2, no. 11, p. a012427–, Nov. 2012.

[23] M. M. Ramsey, K. P. Rumbaugh, and M. Whiteley, “Metabolite cross-feeding enhances virulence in a model polymicrobial infection.,” *PLoS Pathog.*, vol. 7, no. 3, p. e1002012, Mar. 2011.

[24] S. T. Flickinger, M. F. Copeland, E. M. Downes, A. T. Braasch, H. H. Tuson, Y.-J. Eun, and D. B. Weibel, “Quorum sensing between Pseudomonas aeruginosa biofilms accelerates cell growth.,” *J. Am. Chem. Soc.*, vol. 133, no. 15, pp. 5966–75, Apr. 2011.

[25] S. Alberghini, E. Polone, V. Corich, M. Carlot, F. Seno, A. Trovato, and A. Squartini, “Consequences of relative cellular positioning on quorum sensing and bacterial cell-to-cell communication.,” *FEMS Microbiol. Lett.*, vol. 292, no. 2, pp. 149–61, Mar. 2009.

[26] P. A. Lambert, “Mechanisms of antibiotic resistance in Pseudomonas aeruginosa.,” *J. R. Soc. Med.*, vol. 95 Suppl 4, pp. 22–6, Jan. 2002.

[27] M. Kamruzzaman, S. M. N. Udden, D. E. Cameron, S. B. Calderwood, G. B. Nair, J. J. Mekalanos, and S. M. Faruque, “Quorum-regulated biofilms enhance the development of conditionally viable, environmental Vibrio cholerae.,” *Proc. Natl. Acad. Sci. U. S. A.*, vol. 107, no. 4, pp. 1588–93, Jan. 2010.

[28] J. L. Murray, J. L. Connell, A. Stacy, K. H. Turner, and M. Whiteley, “Mechanisms of synergy in polymicrobial infections.,” *J. Microbiol.*, vol. 52, no. 3, pp. 188–99, Mar. 2014.

[29] M. E. Hibbing, C. Fuqua, M. R. Parsek, and S. B. Peterson, “Bacterial competition: surviving and thriving in the microbial jungle.,” *Nat. Rev. Microbiol.*, vol. 8, no. 1, pp. 15–25, Jan. 2010.

[30] K. P. Rumbaugh, S. P. Diggle, C. M. Watters, A. Ross-Gillespie, A. S. Griffin, and S. A. West, “Quorum sensing and the social evolution of bacterial virulence.,” *Curr. Biol.*, vol. 19, no. 4, pp. 341–5, Feb. 2009.

[31] J. W. Schertzer, M. L. Boulette, and M. Whiteley, “More than a signal: non-signaling properties of quorum sensing molecules.,” *Trends Microbiol.*, vol. 17, no. 5, pp. 189–95, May 2009.

[32] G. Yim, H. H. Wang, and J. Davies, “Antibiotics as signalling molecules.,” *Philos. Trans. R. Soc. Lond. B. Biol. Sci.*, vol. 362, no. 1483, pp. 1195–200, Jul. 2007.

[33] M. Wainwright and J. Lederberg, “History of Microbiology ,” in *Encyclopedia of Microbiology, Volume 2* , 1st ed., Salt Lake City, UT: Academic Press, 1992, pp. 419–437.

[34] A. K. Wessel, T. A. Arshad, M. Fitzpatrick, J. L. Connell, R. T. Bonnecaze, J. B. Shear, and M. Whiteley, “Oxygen limitation within a bacterial aggregate.,” *MBio*, vol. 5, no. 2, p. e00992, Jan. 2014.

[35] D. Schleheck, N. Barraud, J. Klebensberger, J. S. Webb, D. McDougald, S. A. Rice, and S. Kjelleberg, “Pseudomonas aeruginosa PAO1 Preferentially Grows as Aggregates in Liquid Batch Cultures and Disperses upon Starvation,” *PLoS One*, vol. 4, no. 5, p. e5513, May 2009.

[36] M. Alhede, K. N. Kragh, K. Qvortrup, M. Allesen-Holm, M. van Gennip, L. D. Christensen, P. Ø. Jensen, A. K. Nielsen, M. Parsek, D. Wozniak, S. Molin, T. Tolker-Nielsen, N. Høiby, M. Givskov, and T. Bjarnsholt, “Phenotypes of non-attached Pseudomonas aeruginosa aggregates resemble surface attached biofilm.,” *PLoS One*, vol. 6, no. 11, p. e27943, Jan. 2011.

[37] P. Stoodley, S. Wilson, L. Hall-Stoodley, J. D. Boyle, H. M. Lappin-Scott, and J. W. Costerton, “Growth and detachment of cell clusters from mature mixed-species biofilms.,” *Appl. Environ. Microbiol.*, vol. 67, no. 12, pp. 5608–13, Dec. 2001.

[38] A. B. Theberge, F. Courtois, Y. Schaerli, M. Fischlechner, C. Abell, F. Hollfelder,

and W. T. S. Huck, “Microdroplets in microfluidics: an evolving platform for discoveries in chemistry and biology.,” *Angew. Chem. Int. Ed. Engl.*, vol. 49, no. 34, pp. 5846–68, Aug. 2010.

[39] L. M. Fidalgo, G. Whyte, D. Bratton, C. F. Kaminski, C. Abell, and W. T. S. Huck, “From microdroplets to microfluidics: selective emulsion separation in microfluidic devices.,” *Angew. Chem. Int. Ed. Engl.*, vol. 47, no. 11, pp. 2042–5, Jan. 2008.

[40] M. T. Guo, A. Rotem, J. A. Heyman, and D. A. Weitz, “Droplet microfluidics for high-throughput biological assays.,” *Lab Chip*, vol. 12, no. 12, pp. 2146–55, Jun. 2012.

[41] J. Q. Boedicker, M. E. Vincent, and R. F. Ismagilov, “Microfluidic confinement of single cells of bacteria in small volumes initiates high-density behavior of quorum sensing and growth and reveals its variability.,” *Angew. Chem. Int. Ed. Engl.*, vol. 48, no. 32, pp. 5908–11, Jan. 2009.

[42] M. Weitz, A. Mückl, K. Kapsner, R. Berg, A. Meyer, and F. C. Simmel, “Communication and computation by bacteria compartmentalized within microemulsion droplets.,” *J. Am. Chem. Soc.*, vol. 136, no. 1, pp. 72–5, Jan. 2014.

[43] E. C. Carnes, D. M. Lopez, N. P. Donegan, A. Cheung, H. Gresham, G. S. Timmins, and C. J. Brinker, “Confinement-induced quorum sensing of individual Staphylococcus aureus bacteria.,” *Nat. Chem. Biol.*, vol. 6, no. 1, pp. 41–5, Jan. 2010.

[44] E. C. Spivey, E. T. Ritschdorff, J. L. Connell, C. A. McLennon, C. E. Schmidt, and J. B. Shear, “Multiphoton Lithography of Unconstrained Three-Dimensional Protein Microstructures,” *Adv. Funct. Mater.*, vol. 23, no. 3, pp. 333–339, Jan. 2013.

[45] R. Nielson, B. Kaehr, and J. B. Shear, “Microreplication and design of biological architectures using dynamic-mask multiphoton lithography.,” *Small*, vol. 5, no. 1, pp. 120–5, Jan. 2009.

[46] S. K. Seidlits, Z. Z. Khaing, R. R. Petersen, J. D. Nickels, J. E. Vanscoy, J. B. Shear, and C. E. Schmidt, “The effects of hyaluronic acid hydrogels with tunable mechanical properties on neural progenitor cell differentiation.,” *Biomaterials*, vol. 31, no. 14, pp. 3930–40, May 2010.

[47] B. Kaehr and J. B. Shear, “Multiphoton fabrication of chemically responsive protein hydrogels for microactuation.,” *Proc. Natl. Acad. Sci. U. S. A.*, vol. 105, no. 26, pp. 8850–4, Jul. 2008.

[48] R. Sunyer, A. J. Jin, R. Nossal, and D. L. Sackett, “Fabrication of hydrogels with steep stiffness gradients for studying cell mechanical response.,” *PLoS One*, vol. 7, no. 10, p. e46107, Jan. 2012.

[49] K. a Mosiewicz, L. Kolb, A. J. van der Vlies, M. M. Martino, P. S. Lienemann, J. a

Hubbell, M. Ehrbar, and M. P. Lutolf, “In situ cell manipulation through enzymatic hydrogel photopatterning.,” *Nat. Mater.*, vol. 12, no. 11, pp. 1072–8, 2013.

[50] P. V. Kozlov and G. I. Burdygina, “The structure and properties of solid gelatin and the principles of their modification,” *Polymer (Guildf).*, vol. 24, no. 6, pp. 651–666, Jun. 1983.

[51] K. Alain and J. Querellou, “Cultivating the uncultured: limits, advances and future challenges.,” *Extremophiles*, vol. 13, no. 4, pp. 583–94, Jul. 2009.

[52] E. J. Stewart, “Growing unculturable bacteria.,” *J. Bacteriol.*, vol. 194, no. 16, pp. 4151–60, Aug. 2012.

[53] M. Göppert-Mayer, “Elementary processes with two quantum transitions,” *Ann. Phys.*, vol. 18, no. 7–8, pp. 466–479, Aug. 2009.

[54] E. Bayer and G. Schaack, “Two-Photon Absorption of CaF2:Eu2+,” *Phys. status solidi*, vol. 41, no. 2, pp. 827–835, 1970.

[55] Szabadvary, *History/Analytical Chemistist*. CRC Press, 1993.

[56] J. B. Shear, “Multiphoton-excited fluorescence in bioanalytical chemistry.,” *Analytical chemistry*, vol. 71, no. 17. p. 598A–605A, 1999.

[57] W. R. Zipfel, R. M. Williams, and W. W. Webb, “Nonlinear magic: multiphoton microscopy in the biosciences,” *Nat. Biotechnol.*, vol. 21, no. 11, pp. 1369–1377, Nov. 2003.

[58] C. Xu, W. Zipfel, J. B. Shear, R. M. Williams, and W. W. Webb, “Multiphoton fluorescence excitation: new spectral windows for biological nonlinear microscopy.,” *Proc. Natl. Acad. Sci. U. S. A.*, vol. 93, no. 20, pp. 10763–8, Oct. 1996.

[59] J. Klein and J. D. Kafka, “The Ti:Sapphire laser: The flexible research tool,” *Nat. Photonics*, vol. 4, no. 5, pp. 289–289, May 2010.

[60] S. Maruo and J. T. Fourkas, “Recent progress in multiphoton microfabrication,” *Laser Photonics Rev.*, vol. 2, no. 1–2, pp. 100–111, Apr. 2008.

[61] J. D. Pitts, P. J. Campagnola, G. a. Epling, and S. L. Goodman, “Submicron multiphoton free-form fabrication of proteins and polymers: studies of reaction efficiencies and applications in sustained release,” *Macromolecules*, vol. 33, no. 5, pp. 1514–1523, 2000.

[62] D. B. Weibel, W. R. Diluzio, and G. M. Whitesides, “Microfabrication meets microbiology.,” *Nat. Rev. Microbiol.*, vol. 5, no. 3, pp. 209–18, Mar. 2007.

[63] H. R. Shen, J. D. Spikes, P. Kopečeková, and J. Kopeček, “Photodynamic crosslinking of proteins. I. Model studies using histidine- and lysine-containing N-(2-hydroxypropyl) methacrylamide copolymers,” *J. Photochem. Photobiol. B Biol.*, vol. 34, no. 2–3, pp. 203–210, 1996.

[64] H. R. Shen, J. D. Spikes, P. Kopečková, and J. Kopeček, "Photodynamic crosslinking of proteins. II. Photocrosslinking of a model protein-ribonuclease A," *J. Photochem. Photobiol. B Biol.*, vol. 35, no. 3, pp. 213–219, 1996.

[65] J. D. Spikes, H.-R. Shen, P. Kopečková, and J. Kopeček, "Photodynamic Crosslinking of Proteins. III. Kinetics of the FMN- and Rose Bengal-sensitized Photooxidation and Intermolecular Crosslinking of Model Tyrosine-containing N-(2-Hydroxypropyl)methacrylamide Copolymers," *Photochem. Photobiol.*, vol. 70, no. 2, pp. 130–137, Aug. 1999.

[66] M. J. Davies and R. J. W. Truscott, "Photo-oxidation of proteins and its role in cataractogenesis," *J. Photochem. Photobiol. B Biol.*, vol. 63, no. 1–3, pp. 114–125, Oct. 2001.

[67] J. D. Pitts, A. R. Howell, R. Taboada, I. Banerjee, J. Wang, S. L. Goodman, and P. J. Campagnola, "New Photoactivators for Multiphoton Excited Three-dimensional Submicron Cross-linking of Proteins: Bovine Serum Albumin and Type 1 Collagen¶†," *Photochem. Photobiol.*, vol. 76, no. 2, pp. 135–144, May 2007.

[68] Christopher S. Foote, *Light-Activated Pesticides*, vol. 339. Washington, DC: American Chemical Society, 1987.

[69] S. C. N. Montoya, L. R. Comini, M. Sarmiento, C. Becerra, I. Albesa, G. A. Argüello, and J. L. Cabrera, "Natural anthraquinones probed as Type I and Type II photosensitizers: singlet oxygen and superoxide anion production.," *J. Photochem. Photobiol. B.*, vol. 78, no. 1, pp. 77–83, Jan. 2005.

[70] M. DeRosa, "Photosensitized singlet oxygen and its applications," *Coord. Chem. Rev.*, vol. 233–234, pp. 351–371, Nov. 2002.

[71] E. B. M. Breidenstein, C. de la Fuente-Núñez, and R. E. W. Hancock, "Pseudomonas aeruginosa: all roads lead to resistance.," *Trends Microbiol.*, vol. 19, no. 8, pp. 419–26, Aug. 2011.

[72] J. A. Driscoll, S. L. Brody, and M. H. Kollef, "The epidemiology, pathogenesis and treatment of Pseudomonas aeruginosa infections.," *Drugs*, vol. 67, no. 3, pp. 351–68, Jan. 2007.

[73] J. L. Burns, J. Emerson, J. R. Stapp, D. L. Yim, J. Krzewinski, L. Louden, B. W. Ramsey, and C. R. Clausen, "Microbiology of sputum from patients at cystic fibrosis centers in the United States.," *Clin. Infect. Dis.*, vol. 27, no. 1, pp. 158–63, Jul. 1998.

[74] J. Thiele, Y. Ma, S. M. C. Bruekers, S. Ma, and W. T. S. Huck, "25th anniversary article: Designer hydrogels for cell cultures: a materials selection guide.," *Adv. Mater.*, vol. 26, no. 1, pp. 125–47, Jan. 2014.

[75] S. E. Darch, S. A. West, K. Winzer, and S. P. Diggle, "Density-dependent fitness benefits in quorum-sensing bacterial populations.," *Proc. Natl. Acad. Sci. U. S. A.*, vol. 109, no. 21, pp. 8259–63, May 2012.

[76] J. L. Connell, M. Whiteley, and J. B. Shear, “Sociomicrobiology in engineered landscapes,” *Nat. Chem. Biol.*, vol. 8, no. 1, pp. 10–13, 2011.

[77] A. E. LaBauve and M. J. Wargo, *Current Protocols in Microbiology*, vol. Chapter 6. Hoboken, NJ, USA: John Wiley & Sons, Inc., 2005.

[78] C. Alvarez-Ortega and C. S. Harwood, “Responses of Pseudomonas aeruginosa to low oxygen indicate that growth in the cystic fibrosis lung is by aerobic respiration.,” *Mol. Microbiol.*, vol. 65, no. 1, pp. 153–65, Jul. 2007.

[79] T. S. Fisher, “Guidelines for Maintaining Cultured Cells,” *Technical Reference Library*, 2015. [Online]. Available: https://www.thermofisher.com/us/en/home/references/gibco-cell-culture-basics/cell-culture-protocols/maintaining-cultured-cells.html. [Accessed: 04-Dec-2015].

[80] E. Gomez, V. E. Santos, A. Alcon, A. B. Martin, and F. Garcia-Ochoa, “Oxygen-Uptake and Mass-Transfer Rates on the Growth of Pseudomonas p utida CECT5279: Influence on Biodesulfurization (BDS) Capability,” *Energy & Fuels*, vol. 20, no. 4, pp. 1565–1571, Jul. 2006.

[81] D. Koley, M. M. Ramsey, A. J. Bard, and M. Whiteley, “Discovery of a biofilm electrocline using real-time 3D metabolite analysis,” *Proc. Natl. Acad. Sci.*, vol. 108, no. 50, pp. 19996–20001, Nov. 2011.

[82] P. S. Stewart, “Diffusion in biofilms.,” *J. Bacteriol.*, vol. 185, no. 5, pp. 1485–91, Mar. 2003.

[83] L. Hall-Stoodley and P. Stoodley, “Biofilm formation and dispersal and the transmission of human pathogens.,” *Trends Microbiol.*, vol. 13, no. 1, pp. 7–10, Jan. 2005.

[84] M. Cloutier, D. Mantovani, and F. Rosei, “Antibacterial Coatings: Challenges, Perspectives, and Opportunities.,” *Trends Biotechnol.*, vol. 33, no. 11, pp. 637–52, Nov. 2015.

[85] S. Chernousova and M. Epple, “Silver as antibacterial agent: ion, nanoparticle, and metal.,” *Angew. Chem. Int. Ed. Engl.*, vol. 52, no. 6, pp. 1636–53, Feb. 2013.

[86] A. Muñoz-Bonilla and M. Fernández-García, “Polymeric materials with antimicrobial activity,” *Prog. Polym. Sci.*, vol. 37, no. 2, pp. 281–339, Feb. 2012.

[87] I. Banerjee, R. C. Pangule, and R. S. Kane, “Antifouling coatings: recent developments in the design of surfaces that prevent fouling by proteins, bacteria, and marine organisms.,” *Adv. Mater.*, vol. 23, no. 6, pp. 690–718, Feb. 2011.

[88] M. V. Graham, A. P. Mosier, T. R. Kiehl, A. E. Kaloyeros, and N. C. Cady, “Development of antifouling surfaces to reduce bacterial attachment,” *Soft Matter*, vol. 9, no. 27, p. 6235, Jun. 2013.

[89] Y. Lai, F. Pan, C. Xu, H. Fuchs, and L. Chi, “In situ surface-modification-induced

superhydrophobic patterns with reversible wettability and adhesion.," *Adv. Mater.*, vol. 25, no. 12, pp. 1682–6, Mar. 2013.